Dynamical seasonal prediction and predictability of Monsoon

In-Sik Kang
Climate Environment System Research Center
Seoul National University
Seoul, 151-742 Korea

Jagadish Shukla
Center for Ocean-Atmosphere-Land Studies
Calverton, MD, USA

Abstract

We present a historical review of the hypothesis of boundary forced predictability of monsoon, its limitations and the challenges in dynamical seasonal prediction of monsoon rainfall. We also present an assessment of the multi-model seasonal predictability of summer-mean precipitation over the Asian Monsoon-Western Pacific region by using 21 year (1979-1999) hindcast predictions of the five models, participating at the Asia-Pacific Economic Cooperation Climate Network (APCN). The five models consist of the current operational seasonal prediction models of NCEP, NASA, JMA, KMA, and SNU. The potential predictabilities of individual models are shown by various methods including the signal to noise ratio and anomaly correlations. Statistical methods for correcting the bias of the model prediction are developed and applied to individual model predictions. It is shown that the statistical correction is effective for enhancing the predictability, particularly for the Asian Monsoon – Pacific region, where the models have large bias. It is shown that a reasonably good seasonal prediction can be achieved when the multi-model predications are combined based on the composite of the individual predictions after applying the statistical correction to each separately.

Although this chapter describes mainly current status of the Tier-two seasonal prediction systems, the present skills of the Tier-one systems, utilizing coupled ocean-atmosphere models, are also examined using the data from Development of European Multi-model Ensemble System for Seasonal-Interannual Prediction (DEMETER). It is shown that the Tier-one system has advantage in producing better seasonal-mean predictions, particularly in the western Pacific and Indian Ocean where air-sea interaction is active during summer. The spatial correlation skill of the DEMETER multi-model ensemble prediction is 0.47 for the monsoon precipitation over the region of 40-180E and 20S-30N.

1. Introduction

1) Historical review

Variations of monsoon rainfall affect agriculture, drinking water, transportation, health, power, and the very livelihood of billions of people living in the monsoon region. It is no surprise therefore that for more than one hundred years several countries have tried to issue long range forecasts of monsoons (India Meteorological Department started issuing long range forecasts of monsoon rainfall in 1886). The operational long range forecasts of monsoon rainfall were based on empirical relationships derived from past observations of atmospheric pressure, temperature and wind. Blanford (1884) was the first one to suggest the use of a surface boundary condition (snowfall over Himalayas in the preceding winter) to predict the summer monsoon rainfall over India.

Charney and Shukla (1977, 1981) presented a conceptual hypothesis for monsoon predictability based on the influence of the boundary forcing at the Earth's surface. A brief historical perspective on this hypothesis is given here. Charney et al. (1977) had conducted AGCM experiments with NASA/GISS AGCM to investigate the influence of changes in albedo on rainfall over Sahel. In these experiments it was found that the summer rainfall variance among the three ensemble members (each member was integrated only for 45 days) was quite small over the Indian monsoon region, indicating that the boundary conditions mainly control the Indian monsoon rainfall. In the same year, Shukla and Misra (1977) had shown empirical evidence of a possible relationship between Arabian sea surface temperature and Indian rainfall, and Shukla (1975) had shown that in the GFDL atmospheric general circulation model (AGCM), specification of (large) positive SST anomalies over the Arabian sea produced increase in monsoon rainfall over India. Hahn and Shukla (1976) revived the Blanford's hypothesis of snow–monsoon relationship by showing, using satellite derived snow cover data, an inverse relationship between the winter season snow cover over Eurasia and the subsequent summer monsoon rainfall over India. These results, combined with the results from the GISS model in which variance of seasonal rainfall among ensemble members was quite small, lead Charney and Shukla (1977, 1981) to propose a hypothesis that predictability of monsoon depends on the influence of boundary conditions at the earth's surface.

The Charney-Shukla hypothesis has been the central paradigm for monsoon predictability research during the past 25 years. However, dynamical models have had large systematic errors in simulating the seasonal mean anomalies associated with changes of boundary conditions, and therefore the potential predictability of summer monsoon rainfall has been relatively low. Whether our inability to capture the boundary forced signals is due to inadequate models and modeling strategies or due to intrinsic limits to the predictability of seasonal mean rainfall because of large natural intraseasonal variability of monsoon remains an open question and a topic of vigorous debate. In the following section we present a critical retrospective of the Charney-Shukla hypothesis and describe the barriers to realizing the potential predictability.

For the influence of the boundary conditions to be useful to predict monsoon rainfall, the following three conditions need to be satisfied: 1. There must be a large and persistent anomaly at the earth's surface, 2. There must be a well defined dynamical mechanism through which changes in the boundary condition will produce a corresponding change in seasonal mean monsoon rainfall, 3. The seasonal mean response (signal) must be sufficiently large and reproducible so that it can be distinguished from the intrinsic variability (noise) of the model due to internal dynamics alone. A large number of model simulations during the past decade with high resolution AGCMs using advanced parameterizations have clearly shown that the internal variability over the monsoon region is much larger than that found by Charney and Shukla. This implies that large member ensembles are needed to distinguish the boundary forced response from internal dynamics variability. If the internal variability is at small spatial scales and at high frequency, large scale spatio-temporal averages (viz seasonal mean over whole India) could be predicted if the boundary forcings were indeed important, and if the models were able to simulate the appropriate physical effects.

The current generation of AGCMs have such large systematic errors in simulating both the mean and the variance of summer monsoon rainfall that it is not possible to conclude whether our current inability to make useful dynamical seasonal prediction is due to lack of boundary forced predictability or inadequacy of the current models and modeling strategies. Recent research work in which model experiments are carried out with coupled ocean-atmosphere models suggests that the prescription of SST anomalies in AGCM experiments is an inadequate modeling strategy because SST anomalies in the Indian Ocean and the adjoining western Pacific Ocean are either forced by the atmosphere or evolve as a strongly coupled ocean-atmosphere process (Wang et al. 2004). If ocean-atmosphere coupling is indeed crucial for the Indian Ocean and western Pacific SST anomalies, predictability of monsoon must be investigated with coupled ocean-atmosphere models, which currently have large systematic errors. The problem is further compounded by the fact that atmosphere-land interactions are also quite important for simulation and prediction of monsoon rainfall. Even if SST anomalies were able to force significant changes in large scale circulation, the local land-atmosphere interaction will modulate the ocean forced remote response and determine the actual changes in rainfall over land. Therefore, realistic models of the total climate system (ocean-land-atmosphere) are required to understand the predictability, and to make useful predictions of monsoon rainfall.

2) Current dynamical seasonal predictions

In spite of many challenges described above, dynamical seasonal predictions using general circulation models have been implemented by several operational centers in recent years. In particular, possible improvement of seasonal prediction has been sought by use of multi-model ensembles to remove the uncertainties associated with the spread of ensemble predictions with different initial conditions and the uncertainties associated with model parameterizations (Krishnamurti et al. 1999; Palmer et al. 2004). This chapter describes the present status of dynamical multi-model ensemble seasonal

prediction system, particularly for the Monsoon precipitation.

In the ensemble simulation, all ensemble members are forced by the same SST but started from slightly different atmospheric initial conditions (Dix and Hunt 1995; Kumar and Hoerling 1995; Stern and Miyakoda 1995; Zwiers 1996; Kang et al. 2004). The basic idea of this approach is that the differences among the ensemble members can be used to quantify the noise due to internal dynamics, whereas the relative similarity between ensemble members can be considered as the atmospheric response to the external forcing. Thus, the ensemble mean (signal) can be considered as the component of the prediction forced by the SST, and the deviation from the ensemble mean as the stochastic internal component of the prediction. In this approach, the potential predictability is measured by the ratio between the externally forced SST signal and the internal noise using a standard statistical tool for this kind of problem: "analysis of variance" (ANOVA), which is detailed in many previous studies (Shukla 1981; Rowell et al. 1995; Rowell 1998).

Recently, attempts also have been made to reduce the uncertainty of models by simply compositing multi-model solutions (Kang et al. 2002) and by using the so-called the "super-ensemble" method (Krishnamurti et al. 1999). The present skill of dynamical seasonal prediction is low, if any postprocessing is not applied. The poor skill is not only due to the atmospheric internal processes but also due to the model's inability in producing the atmospheric responses to external forcings, particularly the SST anomalies. This model bias in the external component arises from imperfect formulation and parameterization of various physical processes in the model. Different parameterizations produce different solutions. Assuming that the errors of those solutions are independent from each other and various model solutions spread randomly but close to the observation, the composite of many model solutions can reduce the model random errors.

The model error can also be reduced by statistical correction methods. A major part of non-systematic error of each model can be corrected by a statistical relationship between the prediction and observed anomalies. Most commonly used methodology is the so-called coupled pattern technique (Graham et al. 1994), based on singular value decomposition (SVD) analysis and canonical correlation analysis (CCA). Ward and Navarra (1997) applied SVD to simultaneous fields of GCM simulated precipitation and observed precipitation to correct the errors in the model response to SST forcing. CCA has been widely used for a statistical seasonal prediction system (Barnett and Preisendorfer 1987; Barnston 1994). A recent study by Feddersen et al. (1999) demonstrated that the postprocessed results are not sensitive to the choice among the methods based on the CCA, SVD, and EOF decompositions. In this paper, the postprocessing procedures of the error correction are developed based on the SVD analysis and a point-wise statistical downscaling method. By comparing the potential predictabilities with and without the correction, we can evaluate how the postprocessing of error correction enhances the predictability in the regions of interest.

At present, the dynamical seasonal prediction procedures are categorized

as Tier-two and Tier-one systems. The Tier-two system treats the atmosphere and the ocean (specifically SST) separately. This system relies on an atmospheric GCM integrated with prescribed (either observed or predicted) SST boundary conditions and atmospheric initial conditions. The potential predictability of the Tier-two systems have been examined internationally by the Seasonal Model Intercomparison Project (SMIP II) initiated by the Climate Variability and Predictability Program (CLIVAR)/Working Group on Seasonal to Interannual Prediction (WGSIP). The purpose of SMIP II is to evaluate the current dynamical seasonal prediction systems in a framework, where the lower boundary conditions are prescribed with the observed SSTs for the 20 years 1979-98. On the other hand, SMIP/Historical Forecast Project (HFP) uses the predicted SST conditions instead of the observed, and therefore the SMIP/HFP evaluates the real seasonal predictability of current operational prediction systems.

The Tier-one system utilizes a coupled ocean-atmosphere model. At present, the climatology of coupled models has large systematic bias. However, as mentioned before, the coupled model has some advantage in simulating the monsoon anomalies particularly in the subtropical western Pacific and Indian Ocean, where air-sea interaction plays an important role in producing seasonal-mean anomalies. Recently, the European community has established the Development of European Multimodel Ensemble System for Seasonal-Interannual Prediction (DEMETER) based on the seven coupled models in European countries (Palmer et al. 2004). The aim of DEMETER is to develop a multi-model Tier-one seasonal prediction system and evaluate the skill of the prediction system. At present, ECMWF produces the seasonal prediction regularly based on the DEMETER. The present chapter also shows the skill of the Tier-one DEMETER system.

Section 2 describes the prediction experiment and the data utilized in the present chapter. The potential predictabilities of Tier-two systems are examined in terms of the signal to noise ratio in Section 3 and in terms of anomaly correlation in Section 4. The potential predictability is defined here as the predictability obtained by prescribing the observed (not predicted) SST boundary conditions in the model. Section 5 introduces a statistical correction method and shows how the prediction skill is improved after the correction. Section 6 shows the potential predictability of various multi-model ensemble prediction systems. In contrast to the potential predictability examined in the previous sections, the real predictabilities are assessed in Section 7 by using a Tier-two system with predicted SSTs and Tier-one systems (DEMETER coupled models). Summary and concluding remarks are given in Section 8.

2. Models and Experiments

The data utilized in the present study are obtained from the Asia-Pacific Economic Cooperation (APEC) Climate Network (APCN). The APCN is aimed at producing and disseminating a multi-model ensemble seasonal prediction based on operational prediction products of APEC member countries. Among

them, used are the dynamical seasonal prediction data produced by Japan Meteorological Agency (JMA), Korea Meteorological Administration (KMA), National Aeronautical Space Agency (NASA), National Centers for Environment Prediction (NCEP), and Seoul National University (SNU), in part of the Seasonal Prediction Model Intercomparison Project (SMIP) II, leaded by the CLIVAR/Working Group of Seasonal to Interannual Prediction. The observed SSTs are prescribed for the integration. Therefore, the SMIP II can estimate the upper bound of seasonal predictability but not the actual predictability. The initial conditions are obtained from their own initialization scheme or the NCEP reanalysis data. See the details of SMIP II at the web page, http://www-pcmdi.llnl.gov/projects/smip/smip2.php. The above models consist of different combination of physical parameterizations, listed and summarized in Table 1. The DEMETER data is also used in the present study. Details of the DEMETER can be found in Palmer et al. (2004) and the participating models of DEMETER are listed in Table 2.

The present study focuses on the predictability of seasonal-mean rainfall for boreal summer. For brevity, hereafter "boreal summer" is abbreviated to "summer." The prediction data of each model consists of 10 members of summer-mean precipitation for the 21 summers of 1979-99, except the NASA and JMA models of 9 and 6 members, respectively. The 10 members were generated with the observed initial conditions at 00Z and 12Z 27-31 May. The horizontal resolution of all data is converted to 2.5^{O} in longitude and 2.5^{O} in latitude. Since the climatological mean precipitation of each model was presented in Kang et al. (2002) and other documentations, we will focus on the deviation (anomaly component) from the 21 year prediction climatology of each model. The anomalies thus obtained do not contain the systematic error of each model climatology. The observed precipitation data for the verification is obtained from the Climate Prediction Center Merged Analysis of Precipitation (CMAP) data set (Xie and Arkin, 1997).

3. Limit of seasonal predictability

In this chapter, the interannual variance of model prediction is decomposed into the external (signal) part, related to the SST forcing, and the internal (noise) part, related to the atmospheric nonlinear internal dynamics, and the theoretical limit of seasonal predictability is examined in terms of the signal to noise ratio. Fig. 1a shows the variance of observed summer-mean precipitation for the 21 years. The spatial pattern of Fig. 1a is similar to that of the climatological summer mean shown in Kang et al. (2002), indicating that large variability appears in the regions of large mean precipitation. Figs. 1b-1f are the corresponding variances of each model. Each model variance is estimated based on predictions of all members for the 21 years, and it will be referred to as the total variance. As in the observation, the spatial distribution of the simulated variance appears to be similar to that of the corresponding climatological mean. But, the magnitudes of the simulated variances are quite different for different models. The NCEP variance is particularly large and about ten times larger than that of the JMA over Indochina, South China and Indian regions. The NCEP model has much larger interannual variances than

the observed, and the JMA model has much less variances in most of the regions, particularly over the Asian monsoon region. The difference among the model variances is partly related to the difference in the mean climatology and to the different combination of model physics. But, it is difficult to identify which model physics is responsible for generating such large differences.

The total variance (σ^2_{TOT}) is divided into the external (σ^2_{SST}) and internal variances (σ^2_{INR}; Rowell, 1996). The ensemble mean is considered as the external component of the prediction forced by the SST forcing, and the deviation from the ensemble mean is the stochastic internal component of the prediction. The internal variance can be expressed as

$$\sigma^2_{INR} = \frac{1}{N(n-1)} \sum_{i=1}^{N} \sum_{j=1}^{n} (x_{ij} - \overline{x_i})^2 \qquad (1)$$

where x is the precipitation, i indicates the individual year, N=21, j is the ensemble member, and n is 6 to 10 for different models. $\overline{x}_i$ is the ensemble mean. The external variance is obtained by the mean square of the deviation of each year's ensemble mean from the climatological mean and with a consideration of bias correction, as in Rowell (1996):

$$\sigma^2_{SST} = \sigma^2_{EN} - \frac{1}{n}\sigma^2_{INR}, \text{ and } \sigma^2_{EN} = \frac{1}{N-1} \sum_{i=1}^{N} (\overline{x_i} - \overline{\overline{x}})^2 \qquad (2)$$

where $\overline{\overline{x}}$ is the climatological mean, $\overline{\overline{x}} = 1/(Nn) \sum_{i=1}^{N} \sum_{j=1}^{n} x_{ij}$. It is noted that the sum of external and internal variances expressed above is equal to the total variance.

Figs. 2a-2e show the external variances of various models, and Figs. 2f-2j the internal variances. The signal to noise ratio, the ratio of the external part to the internal part of corresponding model, is shown in Figs. 2k-2o. All models produce large external variances over the tropical oceans, which are much larger than the internal variance of same model, particularly the ENSO region. This result indicates that the tropical rainfall is less controlled by the atmospheric internal processes and thus predictable for a given SST condition. In the extratropics, on the other hand, the internal variances are bigger than the external variances of the same model (Figs. 2k-2o), and therefore the extratropical atmosphere is more controlled by nonlinear stochastic processes and less predictable.

Over the Asian monsoon-western Pacific region, the external and internal parts appear to be equally important for all models, although some models (JMA, NASA, and SNU) have relatively large values of the signal to noise ratio over the region (Figs. 2k-2o) compared to those of the KMA and NCEP models. It is interesting to note that the internal variance is generally proportional to the external variance. In particular, the large variance of the NCEP model shown in Fig. 1 is partly due to the large internal variance, particularly over the Asian

Monsoon region. On the other hand, the internal variance of the JMA model is very weak. As a result, the JMA model has relatively large values of signal to noise ratio, although its forced variance is significantly weaker than those of the other models. It is also noted that the internal variance is very much model dependent, indicating that the internal variations are not only controlled by the dynamics but also by model physics.

The seasonal predictability is limited by the nonlinear stochastic processes in the atmosphere, shown in terms of the internal variance in Fig. 2. Therefore, the seasonal prediction can not be perfect even though we have a perfect GCM and perfect boundary condition and almost perfect initial conditions. Here, the theoretical limit of seasonal predictability is examined by separating the observation (x) into a signal (x_S) and noise (x_N) parts. The signal is related to the slowly varying boundary conditions. The corresponding model variable is then expressed as $y = y_S + y_N$. Assuming that the model signal $y_S = \alpha x_S + y_e$ as in Sugi (2004), where α is the linear regression coefficient between x_S and y_S and y_e is the model error. Then, the model variable $y = \alpha x_S + y_e + y_N$. The correlation coefficient between the observation and model variable can be expressed as,

$$R = \frac{\alpha V(x_S)}{V(x)^{1/2}(\alpha^2 V(x_S) + V(y_e) + V(y_N))^{1/2}} \qquad (3)$$

where the $V(x)$ is a variance of x. The above equation can be driven by assuming that the signal, noise, and error are independent to each other, and therefore all covariances of $Cov(x_S, x_N)$, $Cov(x_S, y_e)$, $Cov(x_N, y_e)$, $Cov(y_e, y_N)$ and $Cov(x_N, y_N)$ are zero. Then the correlation skill can be maximized by minimizing the model error and the noise part. The noise part can be reduced by the ensemble mean procedure, the mean of many predictions with slightly different initial conditions. The model error can be corrected by statistical correlation methods discussed in Section 5 and by using a multi model composite discussed in Section 6. The theoretical limit of seasonal prediction correlation skill can be expressed as,

$$R_{Limit} = \sqrt{\frac{V(x_S)}{V(x)}} = \sqrt{\frac{\rho}{\rho + 1}} \qquad (4)$$

As in equation (4), the theoretical limit can also be expressed in terms of the signal to noise ratio (ρ). Fig. 3a shows the distribution of R_{Limit} estimated using the SNU AGCM. We can also examine the predictability limit using a hypothetical perfect model (a model with no systematic error). The correlation skill of the perfect model is usually estimated by considering one of the ensemble members as observation and correlating the member with the ensemble-mean of the other members. Fig. 3b shows the distribution of perfect model correlation as estimated with the SNU AGCM. As seen in the figures, the theoretical limit of correlation skill is very similar to the perfect model

correlation. The relatively small amplitude of perfect model correlation in the extratropics is due to the sampling error associated with insufficient number of ensemble members. The zonal means of predictability limit of various models are shown in Fig. 4. The figure indicates that the predictability limit in the tropics is relatively high (correlation skill of about 0.8 – 0.9), but it rapidly drops in the subtropics near 30N and fairly low in the extratropics and polar regions (correlation of about 0.2 – 0.4). These correlation values are the upper limit of the dynamical seasonal prediction skill that can be achieved with a perfect model and perfect boundary conditions.

4. Potential predictability of various models

The potential predictability, defined as the predictability of the model measured with perfect boundary (observed SST) conditions, should be lower than the theoretical limit because of incompleteness of the models. The model error is estimated by the difference between the ensemble mean of model predictions and the corresponding observations. The error variances of each model are shown in Figs. 5a-5e. It is interesting to note that the spatial distributions of the errors for all models are similar. All models produce large systematic errors in the Asian Monsoon region and along the ITCZ. The ratio of the external variance to the error variance is shown in Fig. 5f-5j for individual models. A ratio exceeding one indicates that the prediction signal can be considered to be larger than the error. In the Asian monsoon and western Pacific, all models produce errors which are bigger than the signals. This result indicates the large prediction signals in the monsoon region are biased by poor performance of the models. In the next section, we investigate whether it is possible to make a reliable monsoon prediction, if the systematic errors were corrected.

The prediction skill of each model is measured by using the correlation between the anomalies of the ensemble-mean predictions and the observations for 21 years. Since the observed SST was prescribed in the hindcast predictions, this prediction skill is a measure of potential predictability. Fig. 6 shows global distribution of correlation coefficient between the observed and predicted ensemble-mean precipitation at each grid point for the 21 summers. The correlations of various models are shown in Figs. 6b-6f, and Fig. 6a shows the correlations between the observation and the composite of five models. As expected in the previous section, all models have large correlation over the ENSO region, where the external (forced) variance exceeds the internal variance and the model error variance. In contrast, over the Monsoon region, the correlation skill is very poor for all models. It is noted that the model composite does not help improve the correlation skill. In the subtropical western Pacific and the Atlantic Ocean, all models and the composite have large negative correlation values. The negative correlation in the western Pacific is due to model bias, where the external response has large systematic errors (Fig. 5). Recently, Wang et al. (2004) suggested that the poor simulations of precipitation over the western Pacific is due to the Tier-2 prediction system, where the atmospheric feedback to the ocean does not exist. This provides an additional evidence that the ocean-atmosphere coupled processes are important for the

summer precipitation anomalies in the western Pacific.

The spatial correlation over the Monsoon region (40^{O}-160^{O}E, 20^{O}S-30^{O}N) between the anomalies of the ensemble mean seasonal prediction and the corresponding observed precipitation at each year is shown in Fig. 7. With a few exceptions, all models poorly predict the monsoon precipitation for most of the summers. The model composite shows the correlation values below 0.3 for most of the summers, except the years of 1981, 86 and 87. To examine the SST impact on the monsoon prediction, the SSTs are averaged for the four years of good prediction cases (1981, 86, 87, 90) and for the years of bad prediction cases (1980, 82, 94, 97). The averaged SST anomalies are shown in Fig. 8. Comparison between Figures 8a and 8b clearly demonstrate that the monsoon precipitation is indeed closely related to the SST anomalies, particularly over the oceans surrounding the Asian monsoon region and the eastern tropical Pacific.

5. Prediction skill after error correction

(1) Error correction and verification methods

The model bias in the external component appears in a systematic way in both the climatological mean and the anomaly component. The mean bias can be corrected by subtracting the prediction climatology from the prediction of individual year. The systematic error of the anomaly component is related to incorrect performance of GCM in simulating the anomalies, predominantly forced by the SST anomalies. It is noted that a slight shift of the spatial pattern of model anomaly can result in a substantial drop in skill scores when the skill is measured based on the performance at individual grid-points. Here two statistical correction methods are introduced. The first method is based on the singular value decomposition (SVD) (Ward and Navara 1997; Feddersen et. al. 1999; and Kang et al. 2004). As in Kang et al. (2004), the systematic errors of the predicted anomaly are corrected by replacing the SVD modes of prediction to the corresponding observed modes. The transfer function for the replacement can be constructed as follows,

$$X(x,t) = \sum_{i=1}^{P} \alpha_i Y_i(t) R_i(x) \qquad (5)$$

where, X(x,t) is the corrected field, Y(t) is the time coefficients of the SVD mode for the predicted field, and R(x) is the projection of SVD singular vector onto the observed field. i is the mode number, P the total number of the SVD modes, and α is the correlation coefficient between the time series of the SVD mode of prediction and the corresponding SVD time series of observation. It is noted that before obtaining the SVD modes, the EOF analysis is applied to the predicted and observed anomalies, separately, and the observed and predicted fields are reconstructed by retaining the leading 10 EOF modes of each field. This process filters out small scale anomalies and smoothes the spatial fields.

It is noted that the SVD based correction method can not correct the bias which is not related to leading SVD modes and/or has a local character. Another correction method, used in this chapter, is the so-called "Point-wise Downscaling (PDS)" method which is based on the large-scale patterns of

model variables correlated to a local (grid point) observed precipitation. Once, the model patterns are determined from hindcast prediction data, the local precipitation can be predicted by a linear combination of the predictors obtained by projecting the patterns to the dynamical prediction data. The idea of PDS is similar to the statistical prediction using indices of large scale patterns. The detailed procedure is as follows.

Suppose the predictand and predictor field are $Y(t)$ and $X(\lambda,\phi,t)$, respectively. Here Y is a local observed precipitation and X model predicted variables. λ and ϕ are longitude and latitude, respectively. The spatial pattern of the predictor field associated with the predictand can be expressed as,

$$C(\lambda,\phi) = \overline{Y(t)X(\lambda,\phi,t)} \quad \text{and} \tag{6}$$

$$\hat{C}_i = CW_i, \;\; W_i(\lambda,\phi) = \begin{cases} 1 & \textit{inside window} \\ 0 & \textit{outside window} \end{cases}$$

The over bar denotes the time mean for the hindcast period. The window W specifies the positions of the spatial patterns of predictor field. Once obtaining the patterns ($\hat{C}_i$), a local predictand (the corrected prediction) can be obtained by projecting the patterns to the predictor variables of model predicted data, as in the following equation.

$$Y_C(t) = \frac{1}{k}\sum_{i}^{k}(a_i\left\{\sum_{\lambda,\phi} C(\lambda,\phi)W_i(\lambda,\phi)\cdot X(\lambda,\phi,t)\right\} + b_i) \tag{7}$$

The regression coefficients (a,b) are obtained by minimizing the error variance of Y using the hindcast prediction data. By applying this technique with a cross-validative manner, one can obtain independently corrected forecast ($Y_i(t)$) for a particular ith window. The most important procedure of PDS method is the selection of optimal windows. For this purpose, we generate a large number corrected predictions corresponding to the windows by moving the position and changing the size. The window sizes changed are from 30^O longitude x 20^O latitude (the minimum size) to 120^O longitude x 50^O latitude (the maximum size). The optimal windows are selected by comparing the temporal correlation skill of corrected forecasts for corresponding windows with a double cross validation procedure (Kaas et al. 1996). The final corrected forecast is not determined by a single pattern with the highest cross validated correlation skill but the ensemble mean of several corrections with several different patterns. The correlation coefficient of each pattern is divided into the several categories based on its statistical significance of the correlation between observation and corrected forecast. We uses 6 categories which lower bounds of the significance level are 99.9%, 99%, 97%, 95%, 92.5%, 90%. Among the 6 categories, only the patterns in the category with the highest significance level are used. If there are five patterns in the first category, the final correction is made by the composite of five corrections based on those patterns. In this case, k=5 in the equation (7). If there is no pattern in the first category and the patterns of next category are used and so on. For the correction of predicted precipitation, the predictor variables used here are precipitation and 850hPa temperature.

It is noted that the corrections of prediction toward observation based on

both the SVD and PDS methods lead to loss of variability in absolute magnitude; that is, the corrected field stays close to climatology. Thus, it may be necessary to apply some sort of inflation method to the adjusted field. The most common way of inflation is to multiply the adjusted values by the ratio between the standard deviation of the observations and that of the adjusted values. In the present study, the inflation factor is obtained by combining the common way of inflation and the weighting factor considered by Feddersen et al. (1999) and used by Kang et al. (2004).

(2) Predictability after error correction

The error correction method introduced above is applied to the SNU predictions here and the applicability of the method to the seasonal prediction is examined based on the one model result. It is then applied to the other models in the next section. Before making the correction, we examined how well the SNU model reproduces the EOF modes of precipitation variability over the globe. Figure 9a shows the first eigenvector of observed summer mean precipitation which explains 24.3% of total variance, and Fig. 9c is the predicted counterpart explaining 39.0% of total variance. Both figures are characterized by the east-west seesaw pattern between the anomalies in the tropical central Pacific and Indonesian subcontinent, although the model centers are shifted to the east. Other noticeable differences include sign differences in the subtropical western Pacific and the Indian Ocean eastward from 60E. The poor performance of the model in those regions is already mentioned in the previous section. The time series associated with the eigenvectors, shown in Fig. 9e, vary in a similar way and are related to ENSO SST anomalies. The difference between the model and observed eigenvectors in the subtropical western Pacific and Indian Ocean is due to failure of the model to simulate the responses of ENSO SST anomalies.

The second eigenvector of the observed summer-mean precipitation shown in Fig. 9b explains 15.7% of total variance. The model counterpart, shown in Fig. 9d, shows that the model reproduces the western Pacific center but with much weaker amplitude. It also produces anomalies in other regions in the Pacific and Indian Ocean that are somewhat different from the observations. However, the similarity between the time series associated with observed EOF modes and the corresponding time series of predicted modes provides hope of error correction for the predicted field. The error correction has been done by using equation (5) and the SVD modes, which represent more clearly the coupled modes of observed and predicted fields than the EOF modes do. The two leading SVD singular vectors (not shown) are very similar to the corresponding EOF eigenvectors shown in Fig. 9. The similarity can be expected from Figs. 9e and 9f, where the two time series of the observed and predicted modes vary almost simultaneously, indicating that the two EOF modes are coupled to each other. The first four SVD modes are used for the correction. The fifth and higher modes consist of small scale patterns and explain small fraction of the variance. Sum of the four modes explains 41.2% of the total variance.

Fig. 10a shows the spatial distribution of the correlation coefficient between observations and the corrected seasonal predictions based on the SVD method. The correlation coefficients of corrected prediction are replaced by those without correction, if the former is smaller than the latter. Those locations

are in the central tropical Pacific, where the correlation coefficient of the original prediction (Fig. 3) is already very large. Clearly, in most of the regions, the predictability is much enhanced by the statistical correction. The enhancement of predictability is particularly pronounced in the western Pacific where the correction skill is negative without correction (Fig. 5f) but has relatively large positive values after correction. The correlation skill of the corrected prediction based on PDS is shown in Fig. 10b. Double cross validation procedure is applied to obtain the correlation skill. In the tropics, both correction methods produce similar results. In the subtropics and extratropics, however, the PDS method has a superior ability in correcting the errors, particularly in the western Pacific.

The prediction skill of monsoon precipitation is shown in Fig. 11 in terms of the spatial pattern correlation between the observed and predicted fields of each year for the monsoon domain of 20^{O}S-30^{O}N and 40-160^{O}E. In the figure, the open bar indicates the pattern correlations without correction, and the shaded and black bars indicate those with the corrections based on the SVD and PDS methods, respectively. The predictability is much enhanced by the corrections for most of the years. The 21-year averages of correlation values are 0.24 for the prediction without correction, and 0.37, and 0.42 for the predictions with the SVD and PDS correction methods, respectively. Since the PDS method has a better performance than the SVD method, hereafter all corrections are made based on the PDS method.

6. Multi-model potential predictability

There are several ways of combining the multi-model outputs. The simplest way is a composite. The basic idea of multi-model composite is that the individual model errors can be cancelled among each other by making the composite. However, the multi-model composite may not be necessarily better than the best single model. The superiority condition of the multi-model composite to the best simple model is given here. After normalizing all anomalies with respect to their corresponding variance, the skill score S (here defined as $S = 1 - V(error)/V(obs)$) can be expressed as

$$\begin{aligned} S_S &= 2R - 1 \\ S_M &= 2R_M - r_M \end{aligned} \qquad (9)$$

Where S_S is the skill score of a single model and R is a correlation coefficient between the observation and the single model. S_M is the skill score of multi-model composite, and $R_M = \frac{1}{N}\sum_{i=1}^{N} R_i$ the mean correlation skill of the N models used in the multi-model composite, and $r_M = \frac{1}{N^2}\sum_{i=1}^{N}\sum_{j=1}^{N} r_{ij}$ the mean of inter-model correlations r_{ij}. The above equation indicates that the multi-model composite has a best skill when several best models are chosen to maximize R_M and the models are least dependent from each other to minimize r_M. In reality, the multi-model composite is not necessarily better than the

single (best) model, mainly because of the inter-model dependency. The difference of the skills, $D = S_M - S_S$, can then be expressed as

$$D = (1 - r_M) - 2(R - R_M) \qquad (10)$$

The multi-model composite is better than a single model if D has a positive value. By denoting R_{Best} as the correlation skill of the best model, r_M and $R_{Best} - R_M$ at each grid point are computed using the five model precipitation data, and those values are plotted in Fig. 12. The best model at each grid point is determined by comparing the prediction skills of the five models, obtained based on the 21 year hindcast data. In the figure, the multi-model composite is better than the single best model if the skills of the best model and the multi-model are in the region below the thick line. The figure indicates that the multi-model composite is better than the single best model in most of the grid points, although there are many exceptions.

There are several ways of combining the multi-model outputs other than the composite. After Krishnamurti et al. (1999, 2000), scientists have tried to improve weather and climate forecasts using an approach so called the "superensemble." The skill of superensemble method depends strongly on the post-processing algorithm for the multiple regression of multi model solutions toward observed fields during a training period. For the post-processing, the respective weights for individual models are generated using a multiple regression technique. The conventional superensemble forecast (Krishnamurti et al. 2000) can be constructed by the following formula.

$$S = \overline{O} + \sum_{i=1}^{N} a_i (F_i - \overline{F_i}) \qquad (11)$$

Where, F_i is the i^{th} model forecast, $\overline{F_i}$ is the mean of the i^{th} forecast over the training period, $\overline{O}$ is the observed mean over the training period, a_i is the weighting factor of i^{th} model, and N is the number of forecast models involved. The design of an optimal weighting function for a long-term forecast is a key for the development of multi-model superensemble system. Here, the weighting factors are obtained based on the singular value decomposition (SVD) method proposed by Yun et al. (2003).

In the present section, the multi-model predictions are combined by the three methods: a simple composite (MME1), the superensemble (MME2), and the composite of model predictions after each model prediction corrected by the statistical PDS method (MME3). It is mentioned that the superensemble method is also applied to the predictions after error correction However, the superensemble in this case dose not provide a better skill compared to the composite of the corrected predictions. It may be because of double fitting to the observation: the first fit of the prediction to the observation for the correction and the second fit for the superensemble.

The spatial pattern correlations over the monsoon region for 1979-99 are

obtained by using MME1, MME2, and MME3, and those are plotted in Fig. 13. As shown in Fig. 6b, the composite is not always better than the best individual model prediction, but the average skill of the composite is comparable to that of best individual model. Therefore, the choice of multi-model composite prediction will be generally safe since we do not know the best model for the prediction. On the other hand, the superensemble skill (MME2) appears to be better than that of the best individual model with a few exceptions. But, as shown in the previous section, the prediction skill of individual model after error correction is usually much better than that of the raw prediction. The correlation skill of MME2 appears to be comparable to that of the best individual model after correction. The composite of corrected predictions (MME3) has usually a superior correlation skill than any of the corrected individual models. The MME3, which is the best system among the prediction systems used here, produces the 21 year average correlation skill of 0.51 for the monsoon summer prediction, which has a statistical significance. The correlation skills in other regions and other seasons must be different, and their usefulness should be examined separately. In conclusion, the dynamical monsoon seasonal prediction requires a multi-model system with statistical post processing, which need further research efforts.

7. Coupled model predictability

In the previous sections, the seasonal predictability was investigated using the AGCM simulations with prescribed observed SST condition. However, a real operational prediction should use predicted SST as a boundary condition of model integration. The methods of SST prediction currently being used are a persistence, ocean-atmosphere coupled models, and various statistical models. As indicated in Introduction, however, the Tier-2 system (AGCM simulation with prescribed SST) has a limitation in simulating correctly the atmospheric response to local SST anomaly in the region of active ocean-atmosphere interaction (Wang et al 2004). As in Wang et al., the local ocean-atmosphere relationships in the Tier1 and Tier2 systems are examined here, before showing the real seasonal predictability of Tier-1 systems.

In contrast to a commonly accepted view that warmer SST produces more precipitation in the tropics, Wang et al. showed in their paper that observed summer-mean precipitation over the tropical western Pacific is negatively correlated with the local SST and the atmosphere feedback to the ocean is an important mechanism for determining the western Pacific SST. This atmosphere feedback mechanism is not included in the Tier-2 system. As a result, the Tier-2 system produces wrong precipitation anomalies over the western Pacific, as seen in Fig. 3. Fig. 14a shows the lead-lag relationship (correlation) between the pentad-mean rainfall and SST averaged over the western Pacific of 5-30N and 110-150E for the summer season. The observed relationship shown with a black line indicates that rainfall leads the negative SST anomaly with a lead time of about 10 days. Such a relationship may be due to the reduction of solar radiation with more cloud and the increase of surface fluxes associated with increase of surface wind. This observed relationship is reasonably well simulated with a proto-type ocean-atmosphere coupled model, the AGCM

coupled with an ocean mixed layer. The mixed layer model used here is a slap model with a fixed 50 meter depth and the SST is controlled only by the surface heat fluxes. On the other hand, the Tier-2 AGCM simulations show that the rainfall is weakly positively correlated with the SST. The AGCM used for the two experiments are the same SNU AGCM, and the results strongly suggest to use an ocean-atmosphere coupled model for correct prediction of summer rainfall over the western Pacific. It is noticed that for the winter season, the winter mean precipitation is positively correlated with the SST and the Tier-2 system can mimic the rainfall-SST relationship in the western Pacific (Fig. 14b). The seasonal dependency of atmosphere-ocean feedback deserves a further research.

The local rainfall and SST relationship during summer is further examined using a fully coupled ocean-atmosphere model and the relationship is compared with those of observation and AGCM alone (Fig. 15). The coupled model used here is the one developed at Climate Environment System Research Center of SNU which uses the SNU AGCM coupled with a GFDL MOM2 ocean model and the ocean mixed layer model developed by Noh (2001). Fig. 14 shows the distribution of local correlation coefficient between the summer-mean precipitation and SST at the same grid point for the 21 year observations of 1979-1999 (Fig. 15a), the AMIP AGCM simulation for 1950-1999 (Fig. 15b), and the 25 year simulation of the coupled model (Fig. 15c). Over the ENSO region, all three figures show that the summer-mean precipitation is highly positively correlated with local SST, indicating that the atmosphere directly responds to the SST in the region. Over the western tropical Pacific and extratropical Pacific, on the other hand, the observed relationships are well reproduced by the coupled model but are quite different (having a different sign) from those of the AGCM, again indicating that coupled ocean-atmosphere processes are important for simulating the summer rainfall over the regions.

The coupled model produces the precipitation anomalies in a similar manner as observed. But it does not guarantee a high prediction skill, which can be achieved only if its SST prediction is reasonably good. We now examine the prediction skill of Tier-1 systems using the seven coupled ocean-atmosphere models participated at the DEMETER project, listed in Table 2. Fig. 16 shows the correlation skills of summer-mean SST for the individual models and the multi-model ensemble over the globe. All models have relatively high correlation skill over the tropical Pacific and relatively low in the extratropical oceans. The correlation skill of the multi-model composite, shown in Fig. 16a, is higher than those of individual models in most of regions and particularly high (over 0.8) in the tropical Pacific. The prediction skills of precipitation of the coupled models, shown in Fig. 17, are relatively high in the tropical Pacific but poor in other regions. The skill of the multi-model composite (Fig. 17a) is similar to that of the best model. As expected, the Tier-1 systems produce slightly better prediction skill over the western Pacific compared to the negative correlation skills that the Tier-2 systems produce in the region.

The year-to-year variations of spatial pattern correlation for the monsoon region between the predicted and observed precipitation are shown in Fig. 18. Shaded and dark circles indicate the correlation values of raw and corrected

predictions, respectively. The statistical correction based on the PDS method improves the correlation skill in the most cases. The MME3 multi-model ensemble method (composite of the corrected predictions), shown as the best method among several multi-model ensemble methods treated in Section 5, is now applied to the DEMETER predictions. The solid line in the figure shows year-to-year variations of the spatial pattern correlation between the observed and the MME3 precipitations for the monsoon region. The 21 year average of the MME3 correlation values is 0.47. This value may represent the prediction skill of summer monsoon precipitation, that we can achieve at present.

8. Summary and concluding remarks

The present chapter reviewed the present status of state-of-the-art dynamical seasonal prediction systems and demonstrated possible improvement of the predictions based on statistical correction and combination of several independent predictions. In particular, seasonal predictability of summer-mean precipitation over the Asian Monsoon-Western Pacific region is assessed by using 21 year hindcast predictions of five models for 1979-1999. The five models consist of the operation seasonal prediction models of Japan Meteorological Agency (JMA), Korea Meteorological Administration (KMA), National Aeronautical Space Agency (NASA), National Centers for Environment Prediction (NCEP), and Seoul National University (SNU). The historical prediction data were produced as part of CLIVAR/Seasonal Prediction Model Intercomparison Project II (SMIP II). In this experiment, the SST boundary conditions during the prediction period are prescribed with observed SSTs, and thus the potential predictability has been assessed. The potential predictabilities of individual models and a multi-model ensemble system are shown by various methods including the signal to noise ratio based on the analysis of variance and the anomaly correlations. In addition to the potential predictability of the Tier-2 systems, the real seasonal predictabilities of Tier-one systems are examined based on the coupled model predictions of the DEMETER project.

The signal to noise ratio of seasonal mean precipitation over the monsoon region is lower than those of other tropical regions. In addition to large noise, all Tier-two models produce large systematic errors in the Asian Monsoon region, particularly in the western Pacific. As a result, all models produce very poor correlation skill over the Monsoon region. The model composite prediction does not help to improve the correlation skill. For the subtropical western Pacific and the Atlantic Ocean, all models and the composite show the correlation skills with relatively large negative values. The negative skill in the western Pacific is due to model bias, where the external response has a large systematic error. Recently, Wang et al. (2004) suggested that the poor simulations of precipitation over the western Pacific is due to the two-tier prediction system, where the atmosphere is forced by the prescribed SST, but in nature the ocean-atmosphere coupled processes are active and atmospheric feedback to the ocean, which is missing in the two-tier approach, is important in the western Pacific.

To correct the model bias, statistical methods based on singular value decomposition and a point-wise downscaling method were developed and applied to individual model predictions. It is shown that the statistical correction is effective in enhancing the predictability, particularly for the Asian Monsoon–Pacific region, where the large model bias is included in the forced signal (Kang et al. 2004). The enhancement of predictability is particularly pronounced in the western Pacific where the correction skill is negative without correction but has relatively large positive values after correction. It is shown that the point-wise correction is generally better than the correction with leading SVD modes.

The individual model errors can be reduced by combining multi-model predictions. Theoretical analysis is made for the superiority condition of multi-model composite to the single best model. It is shown that the multi-model composite has a good skill when several best models are chosen and the models are least dependent from each other. The inter-model dependency is a crucial problem at present for the multi-model prediction, whose performance is better than that of the single best model. Seasonal predictability of multi-model ensemble prediction is assessed by using several multi-model methods including simple composite, superensemble, and composite of corrected individual predictions. It is shown that a reasonably good dynamical seasonal prediction can be achieved when we use the multi-model composite after applying the statistical correction to individual predictions.

The multi-model seasonal prediction based on coupled models is also examined by using the hindcast prediction data of DEMETER. It has been anticipated that the Tier-one system often produces large systematic errors, particularly in the extratropical region, compared to those of the Tier-two system with the prescribed SST anomalies obtained from the same Tier-one system. However, this study shows that the Tier-one system can better predict the summer-mean precipitation particularly over the Monsoon-western Pacific region, where the atmosphere-ocean feedback is active. The DEMETER Tier-one systems appear to produce better prediction skills over the globe compared to Tier-two systems with predicted SST (not shown). The spatial correlation skill of the DEMETER MME3 for summer-mean precipitation, the best among the multi-model ensemble systems treated in this chapter, is 0.47 over the monsoon region. These values may represent the summer-mean precipitation prediction skills that we can achieve with dynamical prediction models at present.

Acknowledgments

The authors appreciate the SNU colleagues and students, Dr. Jong-Sung Kug, Ms. Kyung Jin, Mrs. Jin Ho Yoo, Doo-Young Lee, and Ho-Yong Jeong, and Dr. June-Yi Lee at NASA/GSFC, who contributed their works to the materials presented in this Chapter. The present study was supported by the Climate Environment System Research Center at Seoul National University and the Korea Meteorological Administration.

References

Barnett, T. P., and R. Preisendorfer, 1987: Origins and levels of monthly and seasonal forecast skill for United States surface air temperatures determined by canonical correlation analysis. *Mon. Wea. Rev.*, **115**, 1825-1850.

Barnston, 1994: Linear statistical short-term climate predictive skill in the Northern Hemisphere. *J. Climate*, **7**, 1513-1564.

Blanford, H. F., 1884: On the connection of the Himalaya snowfall with dry winds and seasons of droughts in India. *Proc. Roy. Soc*. London. **37**, 3.

Bonan, G. B., 1995: Land-atmospheric interactions for climate system models: Coupling biophysical, biogeochemical and ecosystem dynamical processes. *Remote Sensing of Environment*, **51**, 57-73.

Charney, W. J. Quirk, S.-H. Chow, and J. Kornfield, 1977: A Comparative Study of the Effects of Albedo Change on Drought in Semi–Arid Regions. . *J. Atmos. Sci*., **34**, 1366–1385.

____, and J. Shukla, 1981: Predictability of monsoons. Paper presented at the Monsoon Symposium in New Delhi, India, 1977, and published in the book *Monsoon Dynamics*, Eds., Sir James Lighthill and R. P. Pearce, Cambridge University Press, pp. 99-110.

Chou, M.-D. 1992: A Solar Radiation Model for Use in Climate Studies. *J. Atmos. Sci.* **49**, 762–772.

_____, and M. J. Suarez, 1994: An efficient thermal infrared radiation parameterization for use in general circulation models. NASA Tech. Memo. 104606, 85 pp.

_____, and M. J. Suarez, 1996: A solar radiation parameterization (CLIRAD-SW) for atmospheric studies. NASA Tech. Memo. 104606, 39 pp.

Dix, M. R., and B. G. Hunt, 1995: Chaotic influences and the problem of deterministic seasonal predictions. *Int. J. Climatol*., **15**, 159-164.

Feddersen, H., A. Navarra, and M. N. Ward, 1999: Reduction of model systematic error by statistical correction for dynamical seasonal prediction. *J. Climate*, **12,** 1974-1989.

Graham, N. E., P. Barnett, R. Wilde, M. Ponater, and S. Schubert, 1994: On the roles of tropical and midlatitude SSTs in forcing interannual to interdecadal variability in the winter Northern Hemisphere circulation. *J. Climate*, **7**, 1416-1441.

Hahn, D. and J. Shukla, 1976: An apparent relationship between Eurasia snow cover and Indian monsoon rainfall. *J. Atmos. Sci.*, **33**, 2461-2436.

JMA, 2002: Outline of the Operational Numerical Weather Prediction at the Japan Meteorological Agency, Appendix to WMO Numerical Weather Prediction Progress Report. JMA 157pp

Kaas, E., T.-S. Li, and T. Schmith, 1996: Statistical hindcast of wind climatology in the North Atlantic and northwestern European region. *Climate Res.*, **7**, 97-110.

Kang, K. Jin, B. Wang, K.-M. Lau, J. Shukla, V. Krishnamurthy, S. D. Schubert, D. E. Waliser, W. F. Stern, A. Kitoh, G. A. Meeh, M. Kanamitsu, V. Y. Galin, V. Satyan, C.-K. Park, and Y. Liu, 2002a: Intercomparison of the Climatological variations of Asian summer monsoon precipitation simulated by 10 GCMs. *Climate Dyn.*, **19**, 383-395.

_____, J.-Y. Lee, and C.-K. Park, 2004: Potential predictability of a dynamical

seasonal prediction system with systematic error correction. *J. Climate*, **17**, 834-844.

Koster, R. D., and M. J. Suarez, 1992: Modeling the land surface boundary in climate models as a composite of independent vegetation stands. *J. Geophys. Res.*, **97**, 2697-2715.

Krishnamurti, T. N., C. M. Kishtawal, T. E. LaRow, D. R. Bachiochi, Z. Zhang, C. E. Willford, S. Gadgil, and S. Surendran, 1999: Improved weather and seasonal climate prediction forecasts from multimodel superensemble. Science, 285, 1548-1550.

_____, C. M. Kishtawal, Z. Zhang, T. LaRow, D. Bachiochi, E. Williford, S. Gadgil, and S. Surendran, 2000: Multimodel ensemble forecasts for weather and seasonal climate, *J. Climate*, **13**, 4196-4216

Kumar, A., and M. P. Hoerling, 1995: Prospects and limitations of seasonal atmospheric GCM predictions. *Bull. Amer. Meteor. Soc.*, 76, 335-345.

Kuo, H. L., 1974: Further Studies of the Parameterization of the Influence of Cumulus Convection on Large-Scale Flow. *J. Atmos. Sci.*, **31**, 1232–1240.

Lacis, A. A., and J. Hansen, 1974: A Parameterization for the Absorption of Solar Radiation in the Earth's Atmosphere. *J. Atmos. Sci.* **31**, 118–133.

Nakajima, T., and M. Tanaka, 1986: Matrix formulations for the transfer of solar radiation in a plane-parallel scattering atmosphere. *J. Quant. Spectrosc. Radiant. Transfer*, **35**, 13-21.

Moorthi, S., and M. J. Suarez, 1992: Relaxed Arakawa-Schubert: A parameterization of moist convection for general circulation models. *Mon. Wea. Rev.* **120**, 978-1002.

Palmer, T. N., A. Alessandri, U. Andersen, P. Cantelaube, M. Davey, P. Délécluse, M. Déqué, E. Díez, F. J. Doblas-Reyes, H. Feddersen, R. Graham, S. Gualdi, J.-F. Guérémy, R. Hagedorn, M. Hoshen, N. Keenlyside, M. Latif, A. Lazar, E. Maisonnave, V. Marletto, A. P. Morse, B. Orfila, P. Rogel, J.-M. Terres, and M. C. Thomson, 2004: Development of a european multimodel ensemble system for seasonal-to-interannual prediction (DEMETER). *Bull. Amer. Meteor. Soc*, **85**, 853–872.

Pan, H.-L. and L. Mahrt, 1987: Interaction between soil hydrology and boundary layer developments. *Bound.-Layer Meteor*, **38**, 185-202.

Rowell, D. P., 1998: Assessing potential seasonal predictability with an ensemble of multidecadal GCM simulations. *J. Climate*. **11**, 109-120.

_____, C. K. Folland, K. Maskell, and M. N. Ward, 1995: Variability of summer rainfall over tropical North Africa (1906-92): Observations and modeling. *Quart. J. Roy. Meteor. Soc.*, **121**, 669-704.

Sellers, P. J., Y. Mintz, Y. C. Sud, and A. Dalcher, 1986: A simple biosphere model (SiB) for use within general circulation model. *J. Atmos. Sci.*, **43**, 505-531.

Shukla, J.,1975: Effect of Arabian Sea surface temperature anomaly on Indian summer monsoon: A numerical experiment with GFDL model. *J. Atmos. Sci.*, **32**, 503-511.

_____, 1981: Dynamical predictability of monthly means. *J. Atmos. Sci.*, **38,** 2547-2572

_____, and B. M. Misra, 1977: Relationships between sea surface temperature and wind speed over the central Arabian sea and monsoon rainfall over India. *Mon. Wea. Rev.*, **105**, 998-1002.

Stern, W., and K. Miyakoda, 1995: The feasibility of seasonal forecasts speculated from multiple GCM simulations. *J. Climate*, **8**, 1071-1085.

Sugi, M. 2004: Improving estimation of potential predictability using a multi-model ensemble method. *Proc. Workshop on ensemble methods*, Exeter, U.K., WGSIP/WGNE/WGCM, CLIVAR, 48-49

Wang, B., I.-S. Kang, and J.-Y. Lee, 2004: Ensemble simulations of Asian-Australian monsoon variability during 1997/1998 El Nino by 11 AGCMs. *J. Climate*, **17**, 803-818

Ward, M. N., and A. Navarra, 1997: Pattern analysis of SST-forced variability in ensemble GCM simulations: Examples over Europe and the tropical Pacific. *J. Climate*., **10**, 2210-2220.

Webster, P.J., V.O. Magana, T. N. Palmer, J. Shukla, R.A. Tomas, M. Yanai and T. Yasunari, 1998: The monsoon: Processes, predictability and prediction. *J. Geophys. Res.*, **103**, 14451-14510.

Xie, P., and P. A. Arkin, 1997: Global Precipitation: A 17-year monthly analysis based on gauge observation, satellite estimates and numerical model outputs. *Bull. Am. Meteor. Soc.*, **78**, 2539-2558.

Yun, W. T., L. Stefanova, and T. N. Krishnamurti, 2003 : Improvement of the multimodel superensemble technique for seasonal forecasts. *J. Climate*, **22**, 3834-3840

Zwiers, F. W., 1996: Interannual variability and predictability in an ensemble of AMIP climate simulations conducted with the CCC GCM2. *Climate Dyn.*, 12, 825-848.

Table Captions

Table 1. Description of the five models of APCN used in the present study.

Table 2. Brief description of the seven ocean-atmosphere coupled models of DEMETER.

Figure Captions

Fig. 1. Variances of summer mean precipitation anomalies for the 21years of 1979-1999. (a) CMAP observation precipitation, (b) JMA, (c) KMA, (d) NASA, (e) NCEP, and (f) SNU prediction models. Variance of each model is computed using all ensemble members of 21 year predictions. Contour interval is 1, 3, 6, 12, 24, and 48 mm^2/day^2 and light and dark shadings indicate the variance more than 3 and 12 mm^2/day^2, respectively.

Fig. 2. (a)-(e) External variance of precipitation based on the ensemble average of each year. (f)-(j) Internal variance based on the deviation of individual members from the ensemble average. Contour interval is 1, 3, 6, 12, 24 and 36 mm^2/day^2 and light and dark shadings indicate the variance more than 3 and 12 mm^2/day^2, respectively. (k)-(o) Signal to noise ratio defined by ratio of the forced variance to the free variance. Contour levels are 1, 2, 4, 8, and 16 and the dashed line indicates 0.5. Shading indicates the signal to noise ratio bigger than 1. Each model is marked at the upper-left corner of each panel.

Fig. 3 (a) The spatial distribution of the limit of correlation skill estimated by using SNU AGCM. (b) Same as in (a) except for the perfect model correlation.

Fig. 4 Zonal mean distribution of theoretical limit of correlation skill for five models in the Northern Hemisphere. Each line corresponds to each model.

Fig. 5. (a)-(e) Variance of the systematic error, the difference between the ensemble average of prediction and the corresponding observation. Contour interval is 1, 3, 6, 12, 24, and 36 mm^2/day^2 and light and dark shadings indicate the variance more than 3 and 12 mm^2/day^2, respectively. (f)-(j) Ratio between the variances of ensemble mean and systematic error. Contour levels are 1, 2, 4, and 8 and the dashed line indicates 0.5. Shadings indicates the ratio bigger than 1. Each model is marked at the upper-left corner of each panel.

Fig. 6. Distribution of correlation coefficient between the observed and simulated ensemble-mean precipitation at each grid point. Each model case is marked at the upper-left corner of each panel, and the five model composite case is shown in (a).

Fig. 7. Pattern correlation coefficients between the observed and predicted precipitations over the monsoon region (40^O-160^OE and 20^OS-30^ON). Correlation values of each model and model composite are shown by various marks denoted in the figure.

Fig. 8. (a) Composite SST anomalies for the years of good monsoon prediction, 1991, 97, and 98. (b) Those for the years of poor monsoon prediction, 1980, 82, 96. Selected cases exceed the one standard deviation of correlation coefficient of composite prediction shown as solid line in Fig. 6b. Shadings denote the anomalies that are significant at the 99% level of each grid point (*Student t*-test).

Fig. 9. EOF modes of the observed and simulated ensemble-mean precipitation. (a) and (b) are the observed first and second eigenvectors, (c) and (d) the simulated counter parts. (e) and (f) are the time series associated with the eigenvectors. Solid and dashed lines indicate the observed and simulated time series, respectively.

Fig. 10. As in Fig. 5 except the predicted precipitation of SNU SMIP after

correction of systematic error using (a) SVD and (b) PDS.

Fig. 11. Pattern correlation coefficients between the observed and predicted precipitations of SNU SMIP before (open bar) and after the bias correction by SVD (gray shaded bar) and PDS (black shaded bar) over the monsoon region (40^{O}-160^{O}E, 20^{O}-30^{O}N).

Fig. 12 Distribution of r_M and $R_{Best} - R_M$, which are computed using five model precipitation data. Each dot corresponds to the each grid point. Thick dashed line indicates threshold for superiority of multi model composite to the single best model. Multi model composite is better than the single best model below this line.

Fig. 13. Time series of spatial pattern correlations over the monsoon region (40^{O}-160^{O}E and 20^{O}S-30^{O}N) between the observed and the predicted precipitations of MME1 (dotted line), MME2 (dashed red line), and MME3 (solid blue line). MME1, MME2, and MME3 are the multi-model predictions based on a simple composite, SVD based superensemble, and the composite of correction predictions by PDS, respectively. The open gray dots are spatial pattern correlation values of individual models.

Fig. 14. Lead-lag correlation coefficient between pentad rainfall and SST averaged over Western North Pacific (5^{o}N~30^{o}N, 110^{o}E~150^{o}E) for June-July-August (upper, it covers 31-48 annual pentad) and December-January-February (lower, 1-12 and 68-73 pentad). Black solid line denotes the observed correlation coefficients between pentad CMAP and weekly OISST data during 1982-1999, dotted line denotes AGCM (1950-1999) and gray dashed line is for CGCM (25 years), respectively.

Fig. 15. Local correlation coefficients between JJA rainfall and SST. (a) observation calculated during 1979-1999, (c) AGCM is for 1950-1999, and (c) CGCM is for 25years, respectively.

Fig. 16. Correlation coefficient of summer-mean SST for the multi-model composite (a) and the individual models (b-h) in a Tier-one system of DEMETER over the globe during 1980-1999.

Fig. 17. Correlation coefficient of summer-mean precipitation for the multi-model ensemble (a) and the individual models (b)-(h) in a Tier-one system, DEMETER over the globe.

Fig. 18 The interannual variation of the averaged value of pattern correlation of the individual DEMETER models before (gray) and after the bias correction (black) over the Monsoon region. The think solid line is the spatial pattern correlation of the multi model composite after the correction (MME3).

Table 1. Description of the five models used in the present study.

Institute	Resolution	Physical parameterizations	
JMA	T63L40	Convection	Prognostic Arakawa-Schubert scheme (JMA, 2002)
		Radiation	JMA (2002)
		Land sfc.	Simple Biosphere Model (Sellers et al. 1986)
KMA	T106L21	Convection	Kuo scheme (Kuo 1974)
		Radiation	Lacis and Hansen (1974)
		Land sfc.	Simple Biosphere Model (Sellers et al. 1986)
NASA	2^{o}x2.5^{o}L34	Convection	Relaxed Arakawa-Schubert scheme (Moorthi and Suarez, 1992)
		Radiation	Chou and Suarez (1994, 1996)
		Land sfc.	Mosaic LSM (Koster and Suarez, 1992)
NCEP	T62L28	Convection	Relaxed Arakawa-Schubert scheme (Moorthi and Suarez, 1992)
		Radiation	Chou (1992), Chou and Suarez (1996)
		Land sfc.	OSU two-layer model (Pan and Mahrt, 1987)
SNU	T63L21	Convection	Relaxed Arakawa-Schubert scheme (Moorthi and Suarez, 1992)
		Radiation	2 stream k-distribution scheme (Nakajima and Tanaka, 1986)
		Land sfc.:	NCAR LSM (Bonan, 1995)

Table 2. Simple description of the 7 ocean-atmosphere coupled models used in a tier-one multi-model seasonal prediction system of DEMETER.

Institute	AGCM	Resolusion	OGCM	Resolution
CERFACS	ARPEGE	T63 31 Levels	OPA 8.2	2.0x2.0 31 Levels
ECMWF	IFS	T95 40 Levels	HOPE-E	1.4x0.3-1.4 29 Levels
INGV	ECHAM-4	T42 19 Levels	OPA 8.1	2.0x0.5-1.5 31 Levels
LODYC	IFS	T95 40 Levels	OPA 8.2	2.0x2.0 31 Levels
Meteo- France	ARPEGE	T63 31 Levels	OPA 8.0	182GPx152GP 31 Levels
Met Office	HadAM3	2.5x3.75 19 Levels	GloSea OGCM based on HadCM3	1.25x0.3-125 40 Levels
MPI	ECHAM-5	T42 19 Levels	MPI-OM1	2.5x0.5-2.5 23 Levels

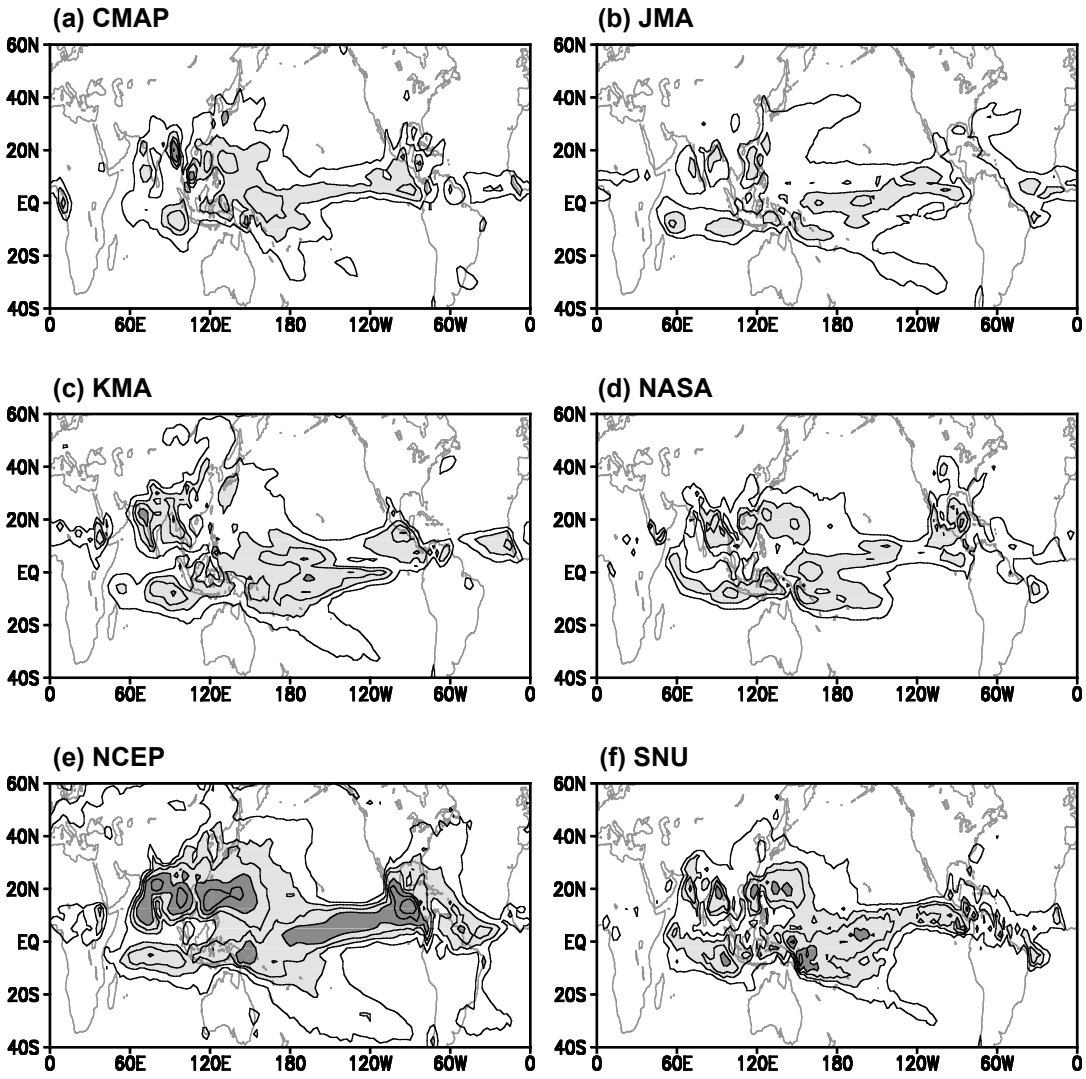

Fig. 1. Variances of summer mean precipitation anomalies for the 21years of 1979-1999. (a) CMAP observation precipitation, (b) JMA, (c) KMA, (d) NASA, (e) NCEP, and (f) SNU prediction models. Variance of each model is computed using all ensemble members of 21 year predictions. Contour interval is 1, 3, 6, 12, 24, and 48 mm^2/day^2 and light and dark shadings indicate the variance more than 3 and 12 mm^2/day^2, respectively.

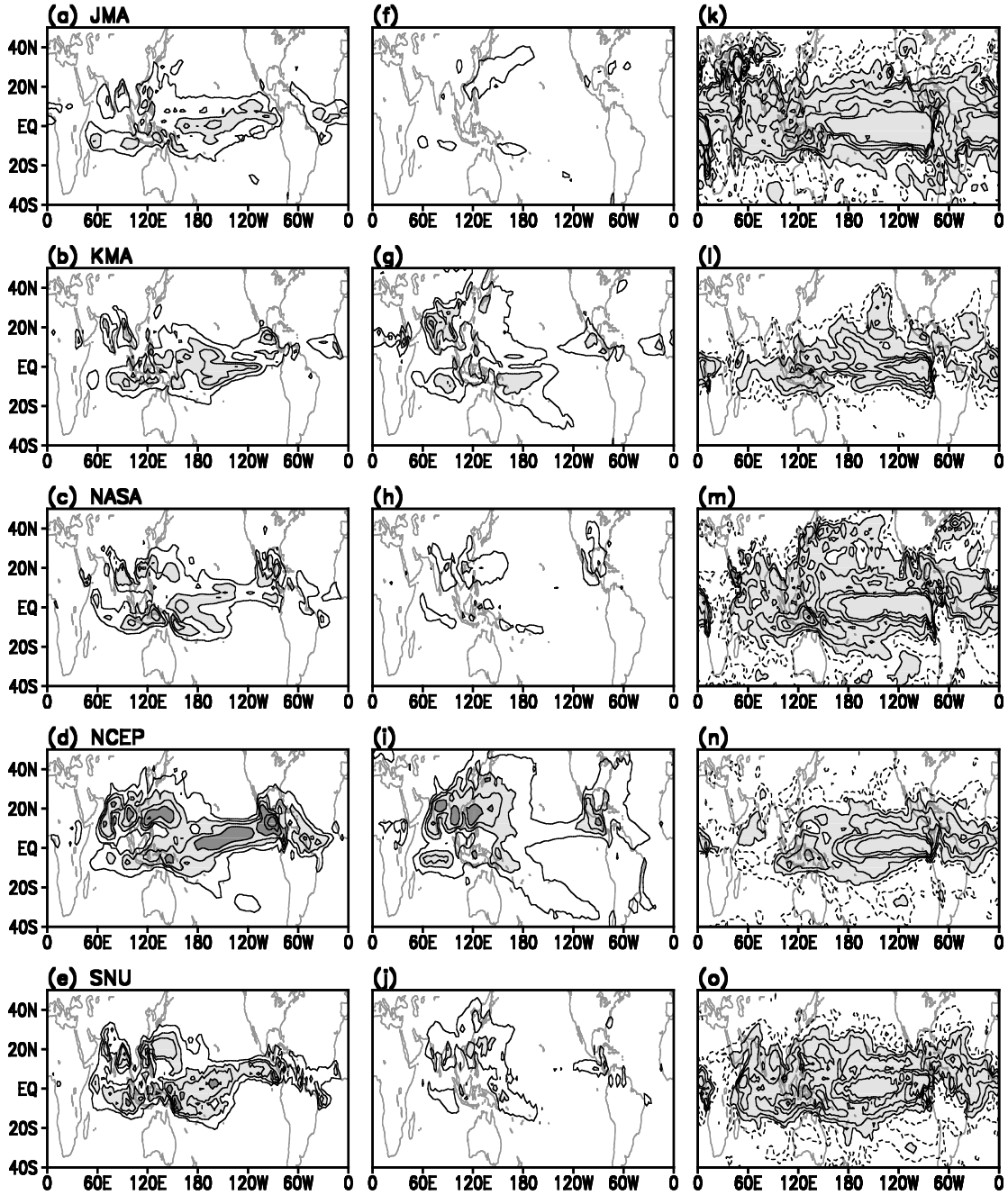

Fig. 2. (a)-(e) External variance of precipitation based on the ensemble average of each year. (f)-(j) Internal variance based on the deviation of individual members from the ensemble average. Contour interval is 1, 3, 6, 12, 24 and 36 mm^2/day^2 and light and dark shadings indicate the variance more than 3 and 12 mm^2/day^2, respectively. (k)-(o) Signal to noise ratio defined by ratio of the forced variance to the free variance. Contour levels are 1, 2, 4, 8, and 16 and the dashed line indicates 0.5. Shading indicates the signal to noise ratio bigger than 1. Each model is marked at the upper-left corner of each panel.

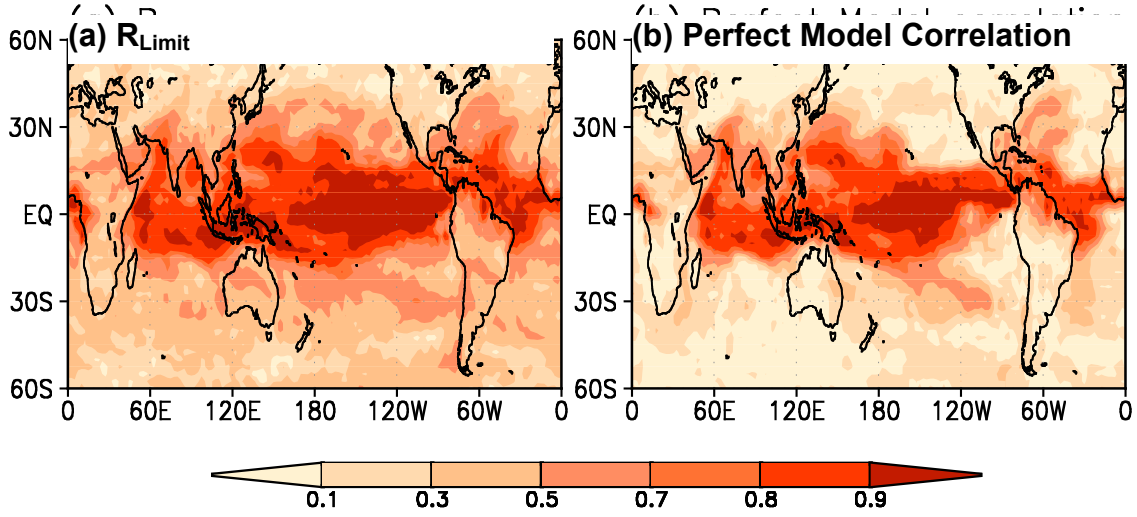

Fig. 3 (a) The spatial distribution of the limit of correlation skill estimated by using SNU AGCM. (b) Same as in (a) except for the perfect model correlation.

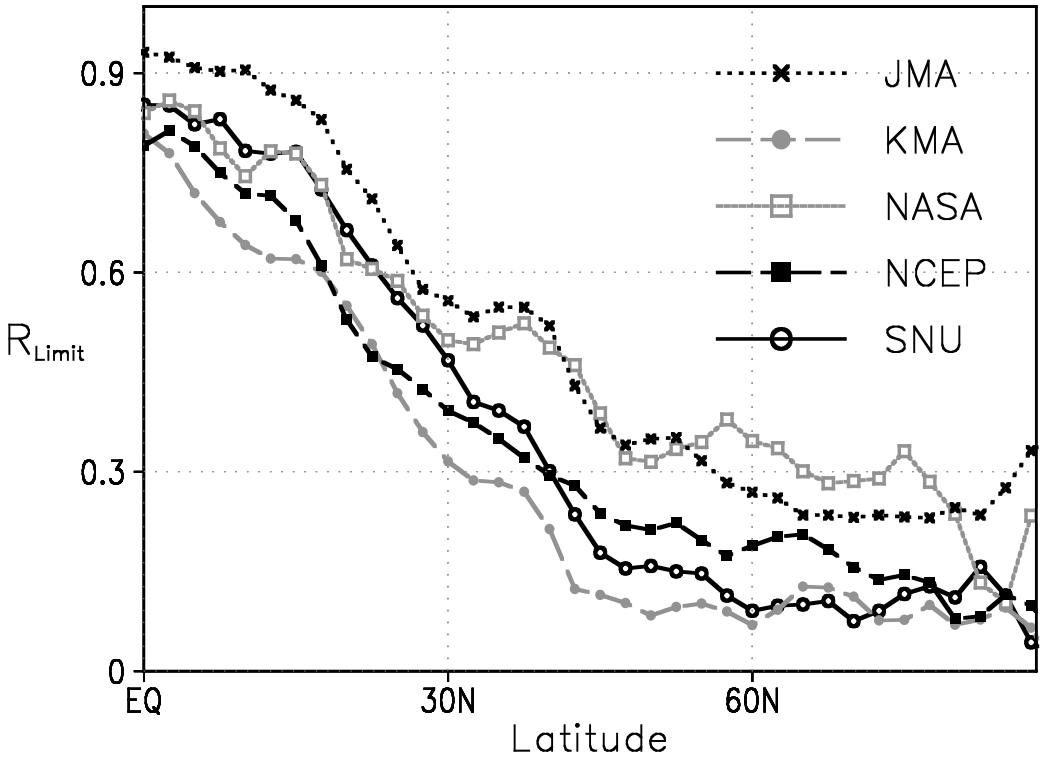

Fig. 4 Zonal mean distribution of theoretical limit of correlation skill for five models in the Northern Hemisphere. Each line corresponds to each model.

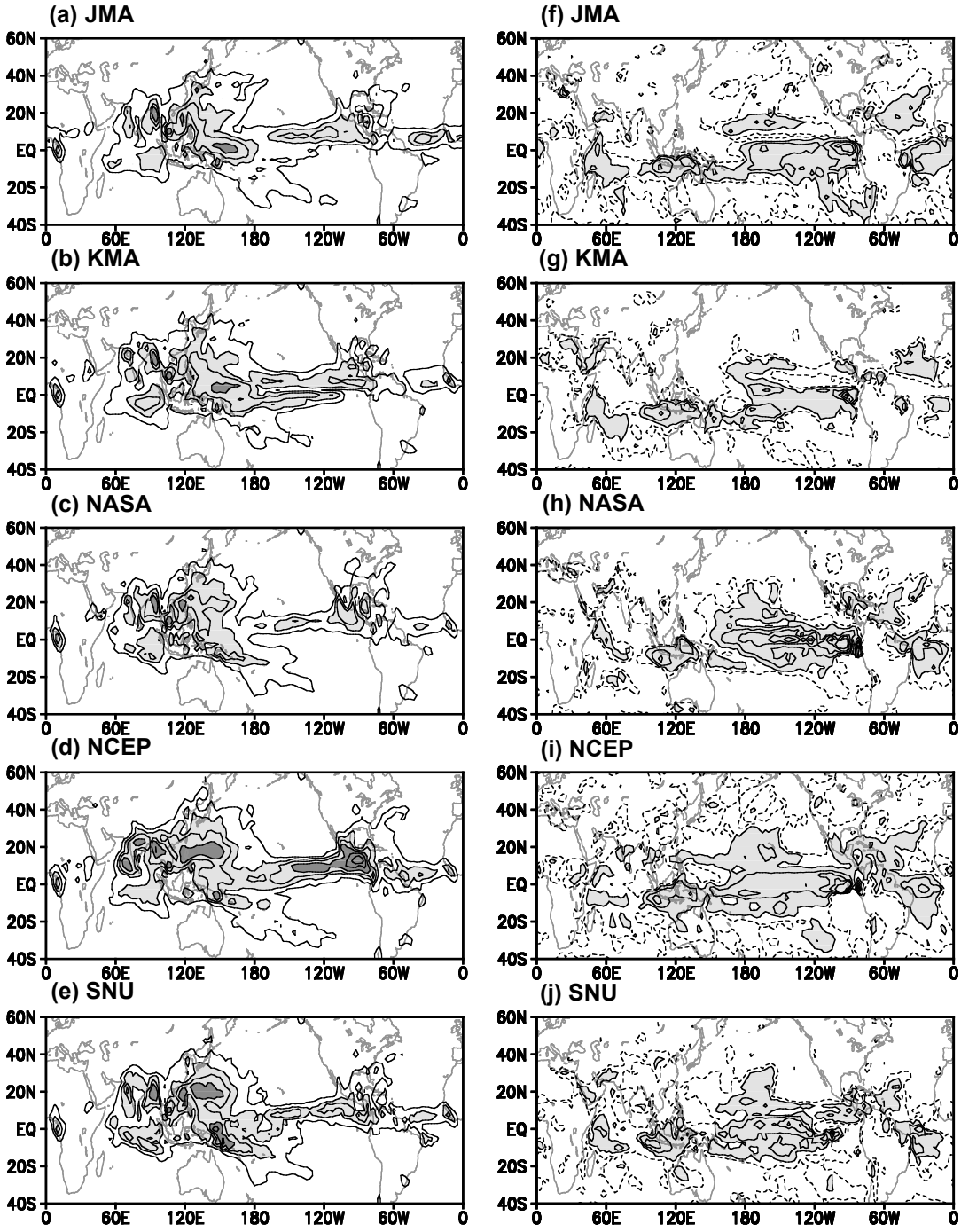

Fig. 5. (a)-(e) Variance of the systematic error, the difference between the ensemble average of prediction and the corresponding observation. Contour interval is 1, 3, 6, 12, 24, and 36 mm^2/day^2 and light and dark shadings indicate the variance more than 3 and 12 mm^2/day^2, respectively. (f)-(j) Ratio between the variances of ensemble mean and systematic error. Contour levels are 1, 2, 4, and 8 and the dashed line indicates 0.5. Shadings indicates the ratio bigger than 1. Each model is marked at the upper-left corner of each panel.

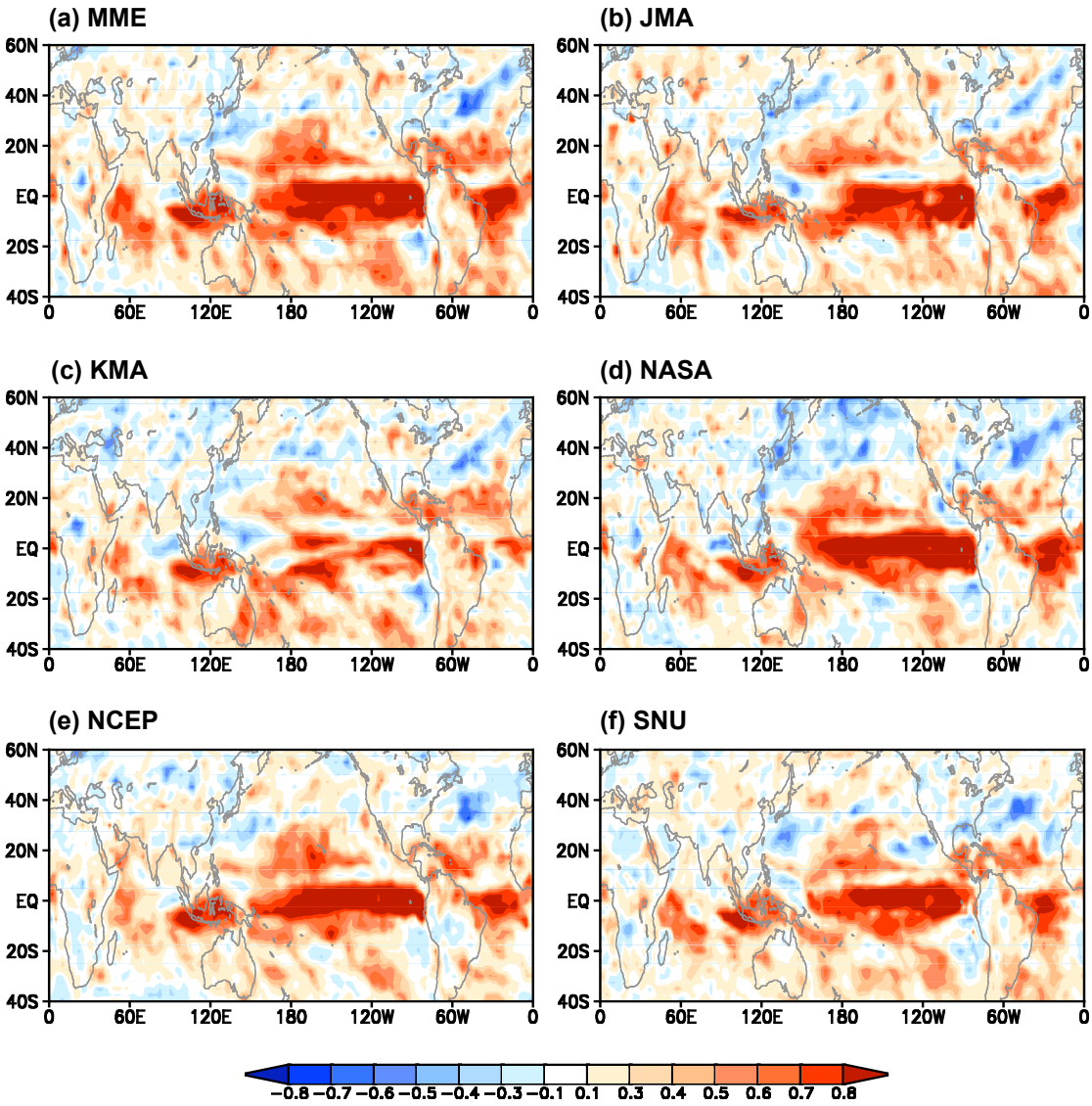

Fig. 6. Distribution of correlation coefficient between the observed and simulated ensemble-mean precipitation at each grid point. Each model case is marked at the upper-left corner of each panel, and the five model composite case is shown in (a).

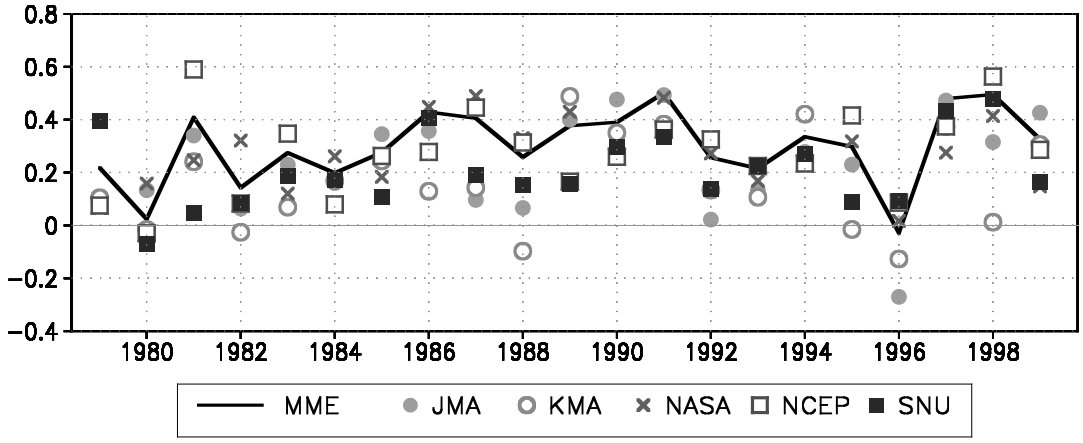

Fig. 7. Pattern correlation coefficients between the observed and predicted precipitations over the monsoon region (40^{O}-160^{O}E and 20^{O}S-30^{O}N). Correlation values of each model and model composite are shown by various marks denoted in the figure.

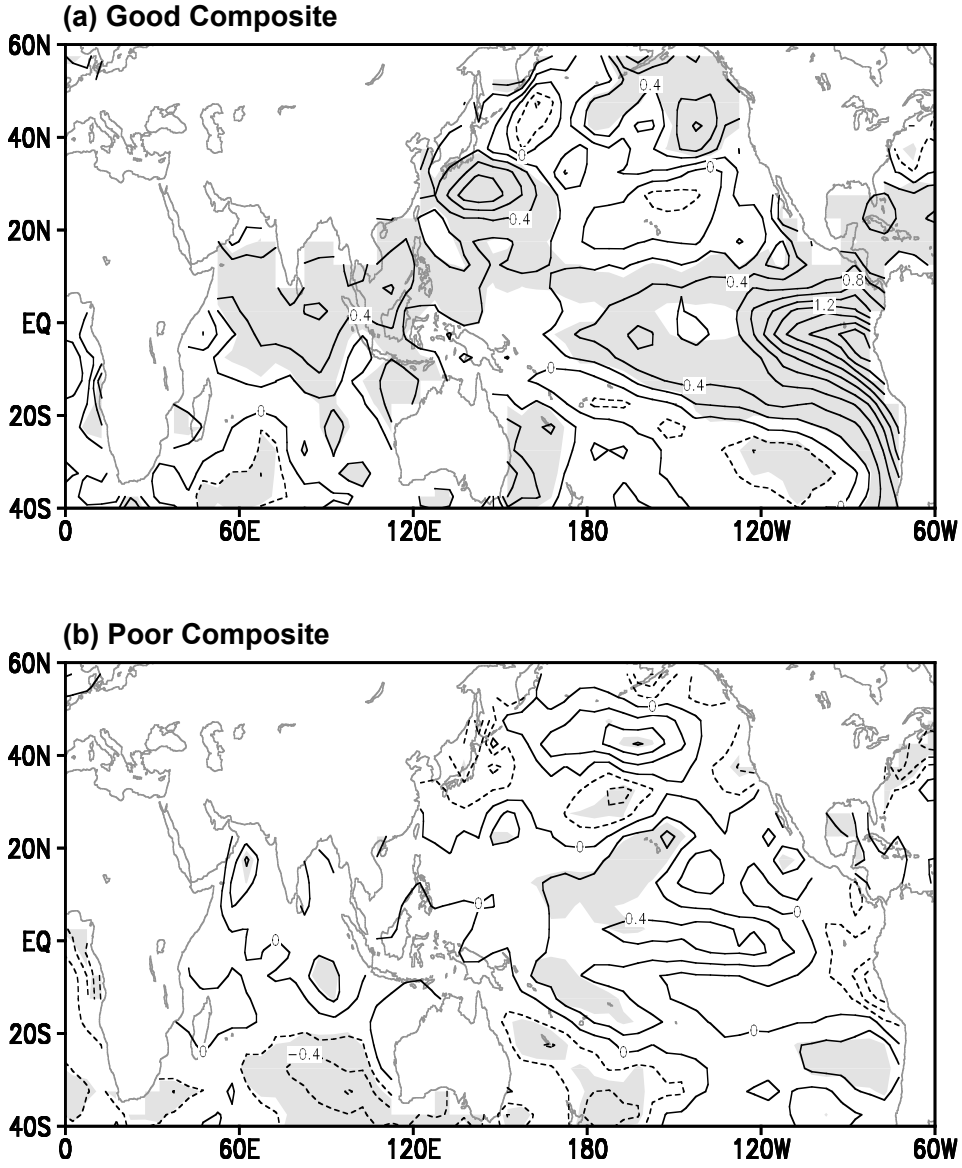

Fig. 8. (a) Composite SST anomalies for the years of good monsoon prediction, 1991, 97, and 98. (b) Those for the years of poor monsoon prediction, 1980, 82, 96. Selected cases exceed the one standard deviation of correlation coefficient of composite prediction shown as solid line in Fig. 6b. Shadings denote the anomalies that are significant at the 99% level of each grid point (*Student t*-test).

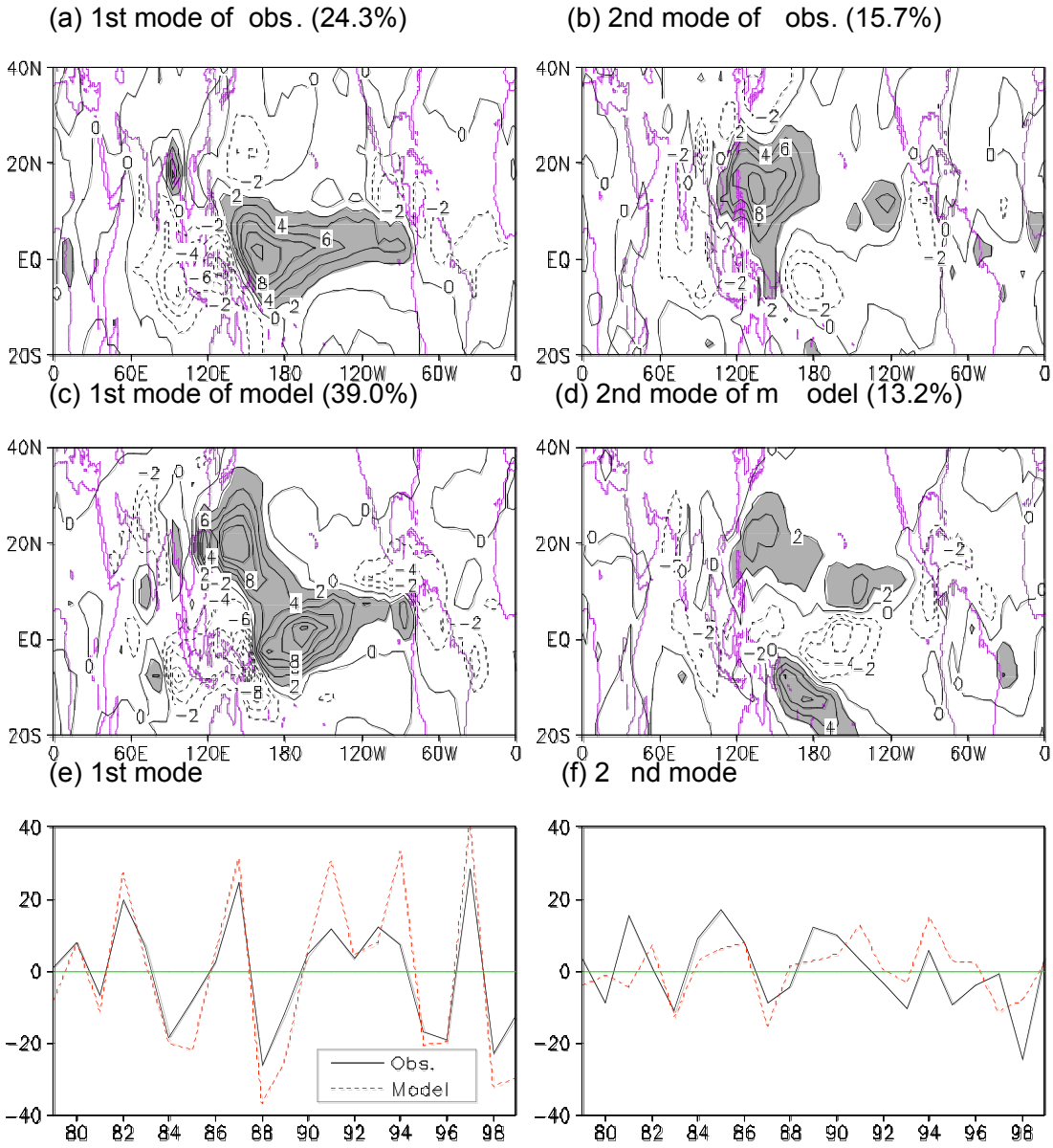

Fig. 9. EOF modes of the observed and simulated ensemble-mean precipitation. (a) and (b) are the observed first and second eigenvectors, (c) and (d) the simulated counter parts. (e) and (f) are the time series associated with the eigenvectors. Solid and dashed lines indicate the observed and simulated time series, respectively.

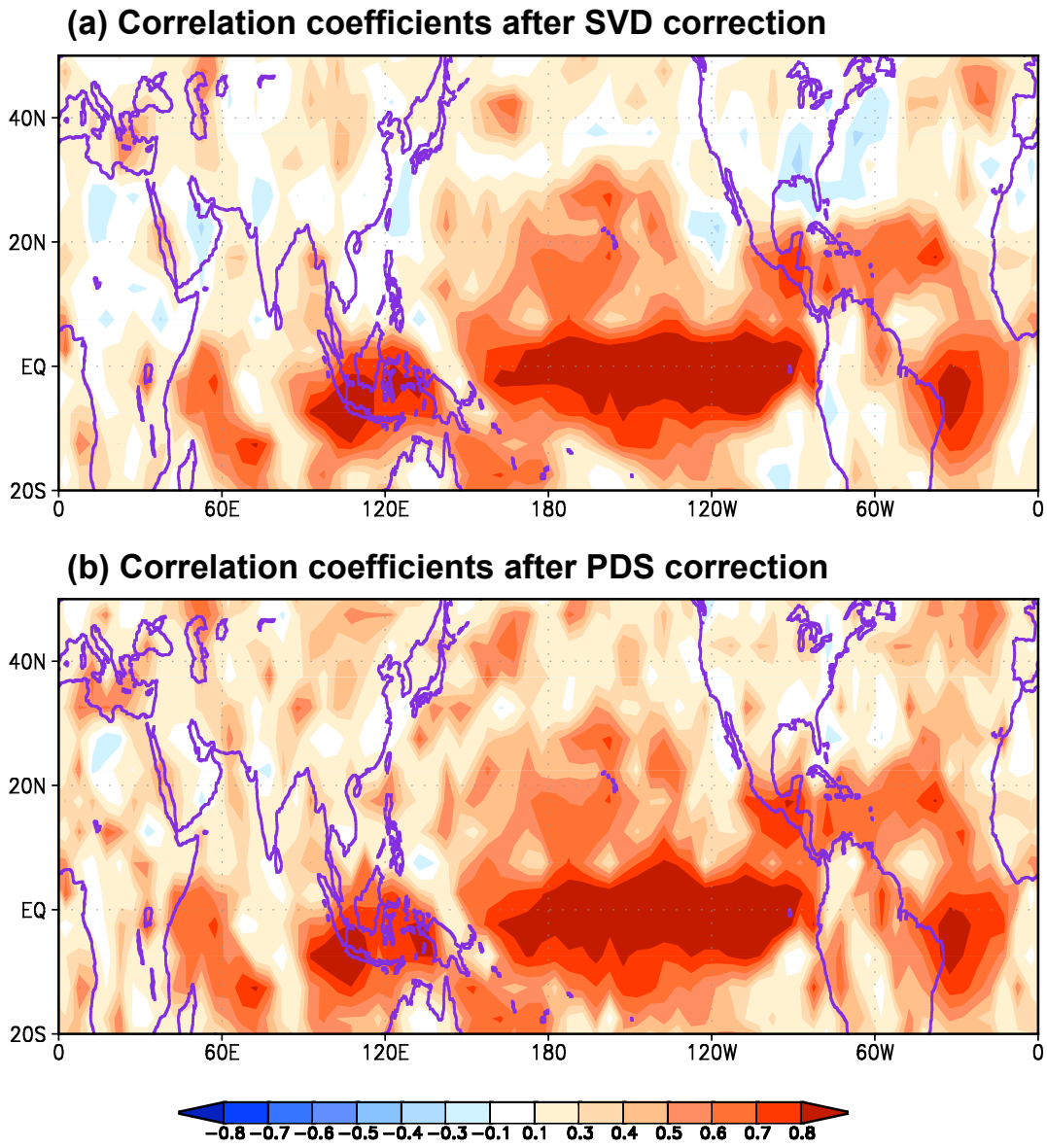

Fig. 10. As in Fig. 5 except the predicted precipitation of SNU SMIP after correction of systematic error using (a) SVD and (b) PDS.

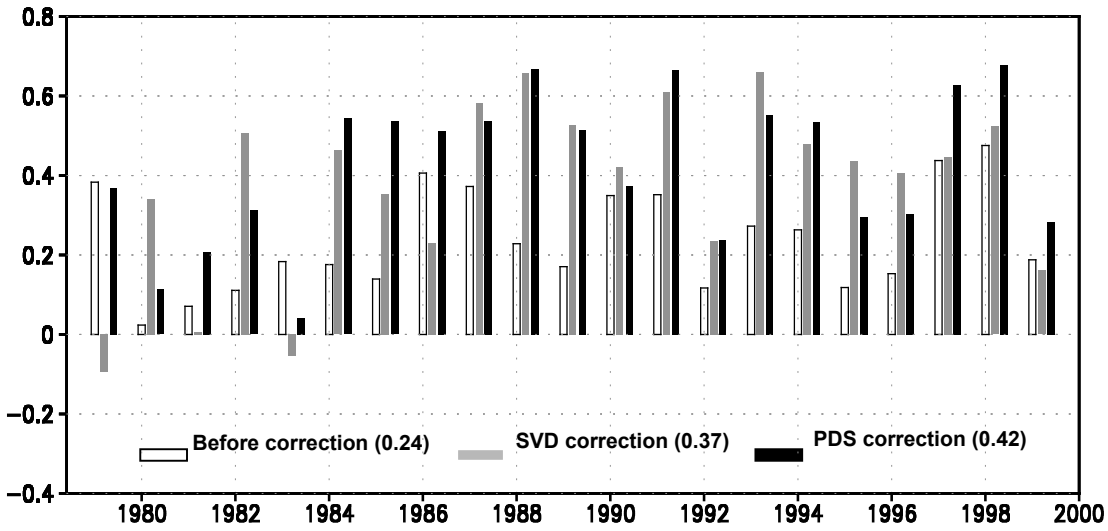

Fig. 11. Pattern correlation coefficients between the observed and predicted precipitations of SNU SMIP before (open bar) and after the bias correction by SVD (gray shaded bar) and PDS (black shaded bar) over the monsoon region (40^{O}-160^{O}E, 20^{O}-30^{O}N).

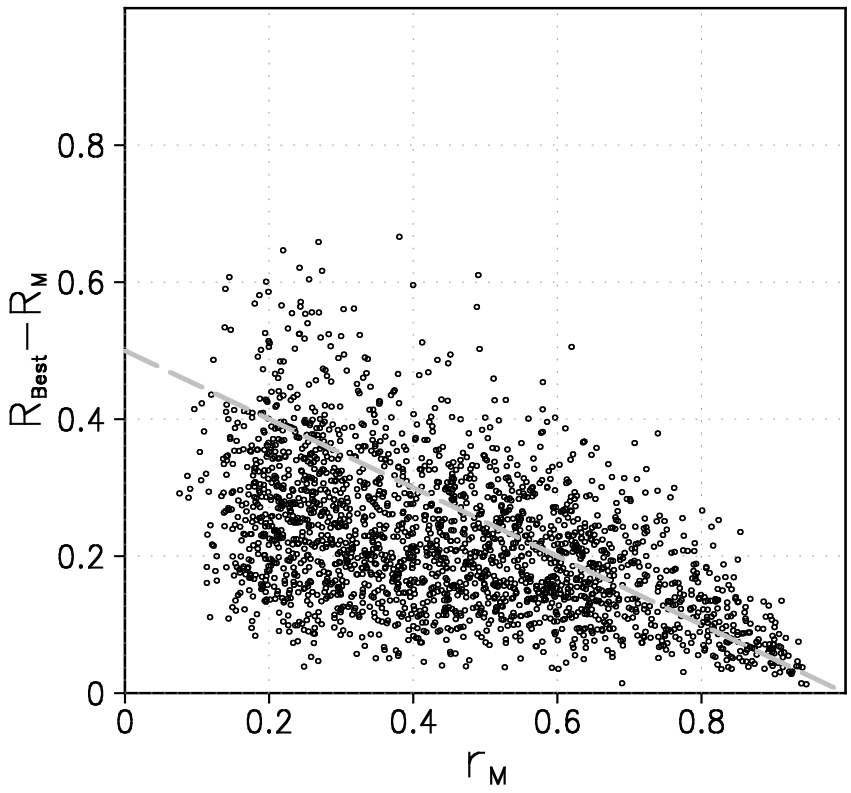

Fig. 12 Distribution of r_M and $R_{Best} - R_M$, which are computed using five model precipitation data. Each dot corresponds to the each grid point. Thick dashed line indicates threshold for superiority of multi model composite to the single best model. Multi model composite is better than the single best model below this line.

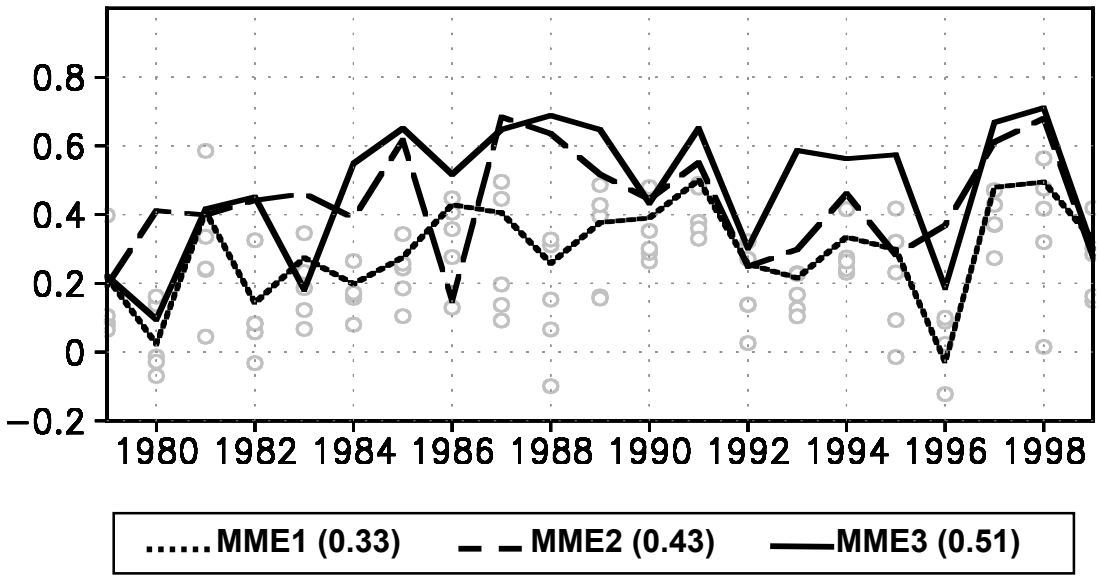

Fig. 13. Time series of spatial pattern correlations over the monsoon region (40^{O}-160^{O}E and 20^{O}S-30^{O}N) between the observed and the predicted precipitations of MME1 (dotted line), MME2 (dashed red line), and MME3 (solid blue line). MME1, MME2, and MME3 are the multi-model predictions based on a simple composite, SVD based superensemble, and the composite of correction predictions by PDS, respectively. The open gray dots are spatial pattern correlation values of individual models.

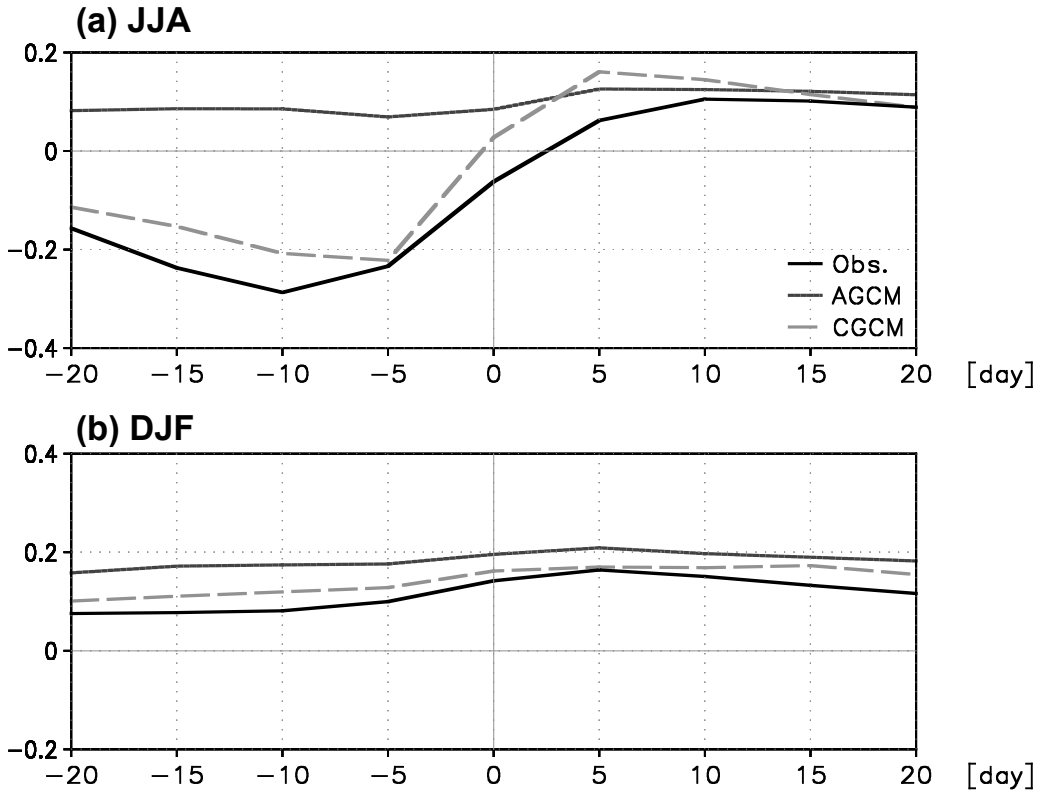

Fig. 14. Lead-lag correlation coefficient between pentad rainfall and SST averaged over Western North Pacific (5°N~30°N, 110°E~150°E) for June-July-August (upper, it covers 31-48 annual pentad) and December-January-February (lower, 1-12 and 68-73 pentad). Black solid line denotes the observed correlation coefficients between pentad CMAP and weekly OISST data during 1982-1999, dotted line denotes AGCM (1950-1999) and gray dashed line is for CGCM (25 years), respectively.

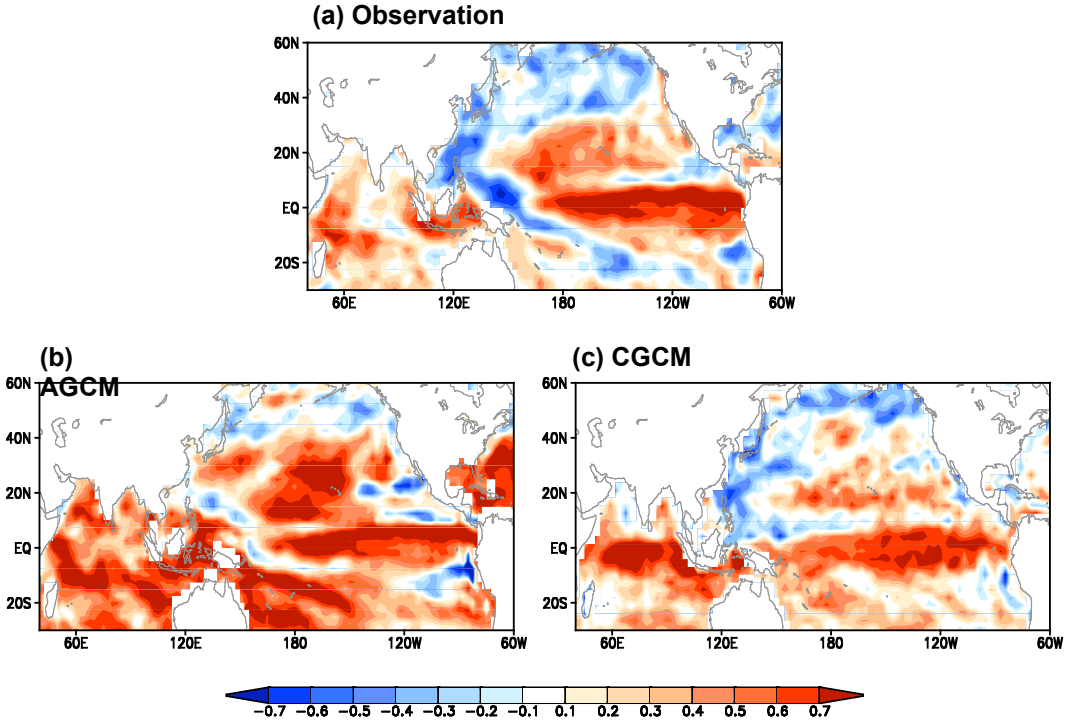

Fig. 15. Local correlation coefficients between JJA rainfall and SST. (a) observation calculated during 1979-1999, (c) AGCM is for 1950-1999, and (c) CGCM is for 25years, respectively.

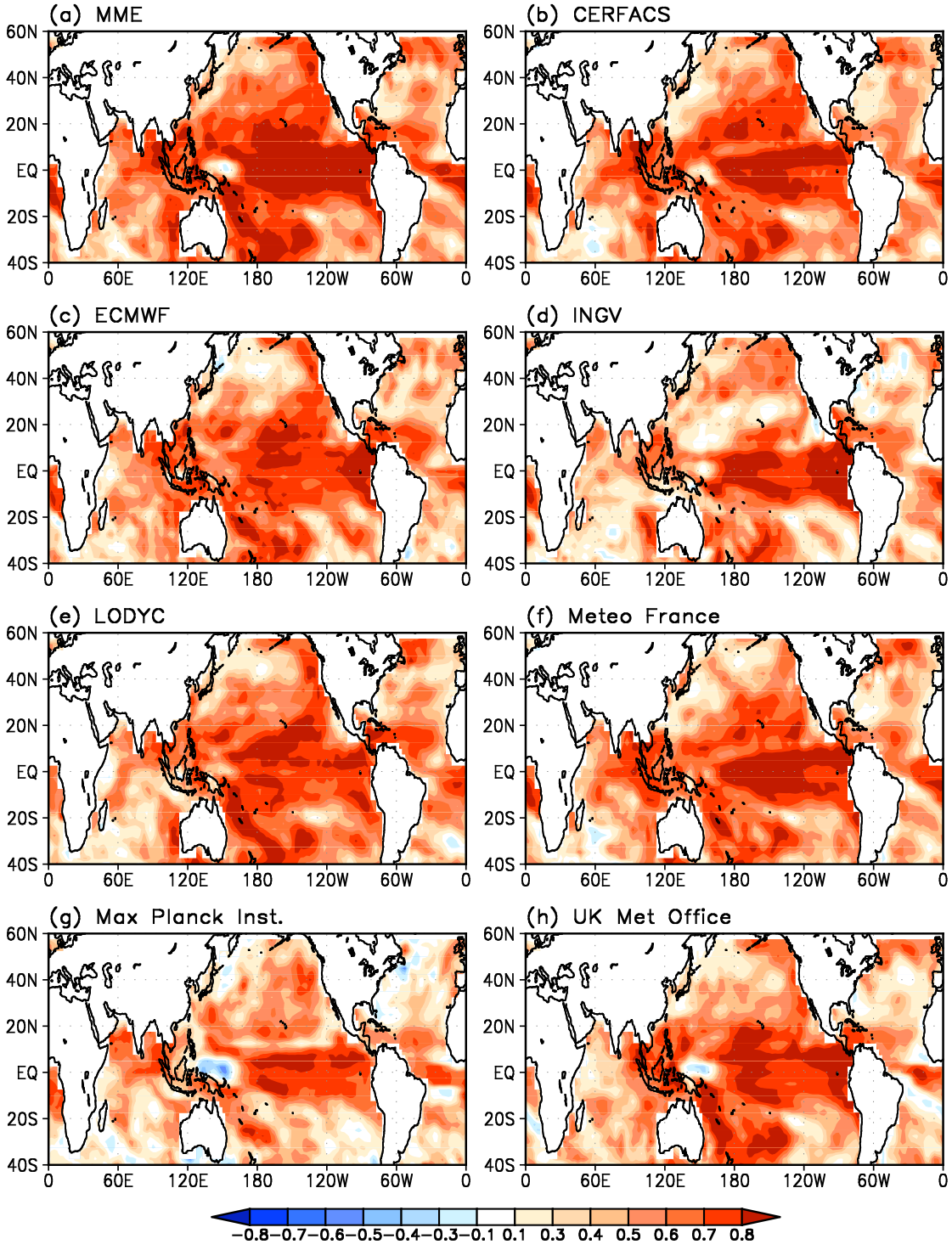

Fig. 16. Correlation coefficient of summer-mean SST for the multi-model composite (a) and the individual models (b-h) in a Tier-one system of DEMETER over the globe during 1980-1999.

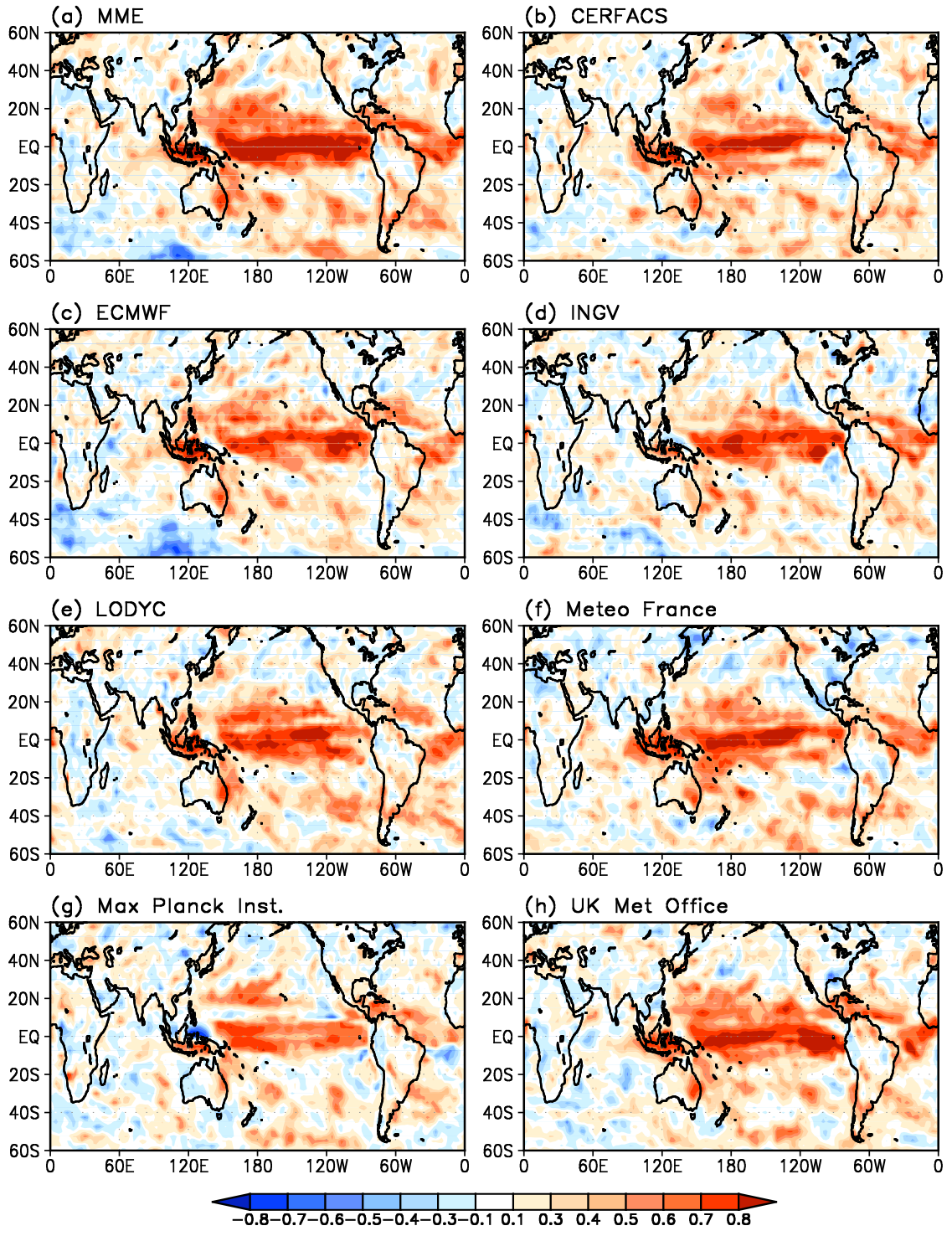

Fig. 17. Correlation coefficient of summer-mean precipitation for the multi-model ensemble (a) and the individual models (b)-(h) in a Tier-one system, DEMETER over the globe.

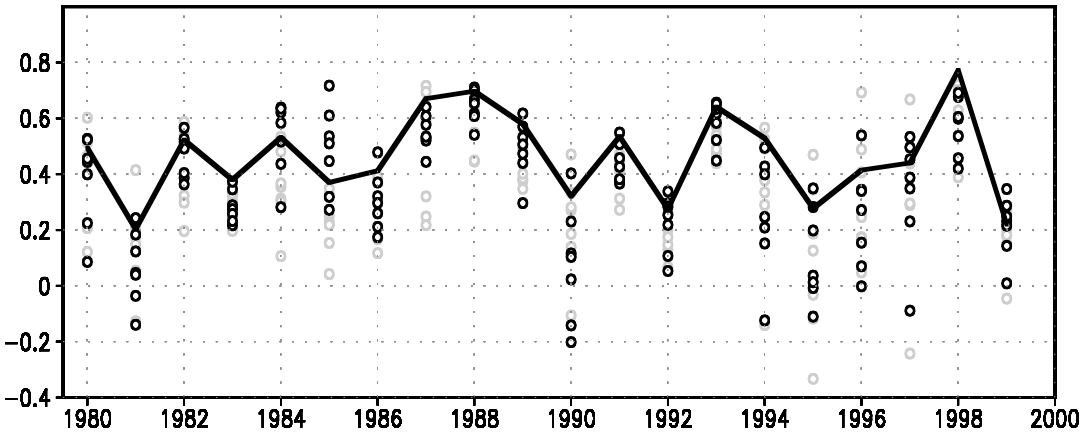

Fig. 18 The interannual variation of the averaged value of pattern correlation of the individual DEMETER models before (gray) and after the bias correction (black) over the Monsoon region. The think solid line is the spatial pattern correlation of the multi model composite after the correction (MME3).